Stress fields of ancient seismicity recorded in the dynamic geometry of pseudotachylyte in the Outer Hebrides Fault Zone, UK

L.R. Campbell[a,b]*, G.E. Lloyd[a], R.J. Phillips[a], R.C. Walcott[c], R.E. Holdsworth[d]

a School of Earth and Environment, University of Leeds, LS2 9JT, UK

b Present address: School of Geography, Earth and Environmental Sciences, Plymouth University, PL4 8AA, UK.

c National Museums Scotland, Chambers Street. Edinburgh, EH1 1JF, UK

d Department of Earth Sciences, Durham University, DH1 3LE, UK

LC ORCiD: 0000-0003-0337-0712

* Corresponding author (lucy.campbell@plymouth.ac.uk)

Abbreviated title: Stress fields recorded in pseudotachylyte

15 Abstract

16 Heterogeneous sequences of exhumed fault rocks preserve a record of long-term evolution of fault
17 strength and deformation behaviour during prolonged tectonic activity. Along the Outer Hebrides
18 Fault Zone (OHFZ), UK, numerous pseudotachylytes record palaeoseismic slip events within
19 sequences of mylonites, cataclasites and phyllonites.

20 To date, the kinematics and controls on seismicity within the long active history of the OHFZ have
21 been poorly constrained. Additional uncertainties over the relative location of a meteorite impact
22 and possible pre-OHFZ brittle faulting also complicates interpretation of the diffuse seismic record.
23 This study presents kinematic analyses of seismicity in the OHFZ, combining observations of offset
24 markers, en-echelon injection veins, and injection vein geometry to reconstruct slip directions and
25 stress fields. This new dataset indicates that a range of fault orientations, slip directions and slip
26 senses hosted seismicity in the OHFZ. Such complexity requires several stress field orientations, in
27 contrast to NW-SE Caledonian compression traditionally attributed to frictional melting along the
28 OHFZ, indicating that seismicity had a long-term presence across the fault zone. Persistence of
29 strong frictional failure alongside the simultaneous development of weak fault rocks and phyllonitic
30 shear zones in parts of the OHFZ has significant implications for understanding seismic hazard along
31 mature continental faults.

32 Supplementary material is available at:

33

Pseudotachylytes are solidified frictional melts generated by seismic rupture along sliding surfaces (Philpotts, 1964; Sibson, 1975; Maddock, 1983; Cowan, 1999, Rowe et al. 2018). In non fault-slip related contexts they may also be generated by impact cratering (e.g. Spray, 1998) or along the frictionally sliding base of large landslides (e.g. Legros et al., 2000). Fault-generated pseudotachylytes, however, are particularly useful in that they record a snapshot of coseismic behaviour along a fault, and are widely accepted to be fault rocks that unequivocally demarcate seismicity (Rowe and Griffith, 2015). In the structural record of long-lived and reactivated fault zones, pseudotachylytes provide useful markers for the location, kinematics and timing of seismic activity. Pseudotachylytes from the Outer Hebrides Fault Zone (OHFZ), Scotland (Fig. 1), were first used for seismic analysis by Sibson (1975, 1977a, 1980), and the fault zone has since become a classic area for this fault rock type (Macaudière and Brown, 1982; Maddock, 1983; White, 1996; MacInnes et al., 2000; Osinski et al., 2001). The OHFZ is a crustal-scale fault (Smythe et al., 1982) traditionally thought to have accommodated significant Caledonian convergence within the basement of the Laurentian foreland to the orogenic belt (Streule et al., 2010). However, the fault zone has in fact accommodated a larger range of movement over its active history in addition to thrusting, including late strike-slip movement and subsequent extension as the Caledonian orogeny progressed (Butler et al., 1995; Imber et al., 2001; Szulc et al., 2008). Additionally, the earliest movement on the OHFZ may have initiated as ductile thrusting at a much earlier date, at around 1100 Ma (see Imber et al., 2002 for discussion).

It is not always clear whether the seismicity indicated by OHFZ pseudotachylytes was associated with Caledonian thrusting, as initially envisaged by Sibson (1975). Fault orientations (Fig. 1) and slip directions on pseudotachylyte-bearing faults in the OHFZ are not always consistent with top-to-the NW reverse movements typically attributed to Caledonian compression (White and Glasser, 1987; MacInnes et al., 2000; Osinski et al., 2001). Further observations are needed to fully investigate whether seismicity across the OHFZ, recorded by pseudotachylytes with observed fault lengths typically < 10 m, occurred predominantly within one kinematic phase (such as Caledonian thrusting)

with additional accommodation of movement on smaller secondary normal and/or strike-slip faults, or whether multiple regional-scale kinematic regimes and associated stress fields triggered seismicity throughout the active history of the OHFZ.

Major fault zones are typically considered to progressively decrease in strength after repeated periods of slip and the associated onset of weakening mechanisms such as grain size reduction and mineral phase changes (Imber et al., 1997; Collettini et al., 2009; Holdsworth et al., 2011; Behr and Platt, 2014). Constraining the timing of active seismicity, controlled by this evolution of fault strength, is an important concept in understanding where earthquakes may continue to nucleate along mature faults that otherwise appear to be creeping aseismically and hence are assumed to be weak. In the case where seismicity occurs along well-established fault zones, different spatial distributions of seismic and aseismic behaviour have been proposed, with earthquake nucleation restricted to either deeper locked sections beneath the aseismic portion (e.g. Wallis et al., 2013) or along fault segments that have escaped spatially heterogenous fault weakening processes such as fluid influx (e.g. MacInnes et al., 2000).

Despite the abundance of pseudotachylyte-bearing faults in the OHFZ (Sibson, 1975), the magnitudes of displacement and senses of slip are often difficult to determine due to the rarity of identifiable offset markers. As a result, the kinematic context and timing of seismicity on the OHFZ has remained rather poorly constrained. Here we supplement field offset marker observations with data derived from a range of kinematic indicators inherent to the geometry of pseudotachylyte fault networks, including fault orientation and injection veins related to dynamic tensile fracturing, in order to assess the kinematic regime(s) recorded by the OHFZ pseudotachylytes. In doing so, we aim to better constrain the seismic environment of this ‘classic’ area and to explore the history of seismicity in relation to the development and maturation of a crustal scale fault.

Geological Background

The OHFZ is exposed for almost 200 km onshore along the eastern seaboard of the Outer Hebrides (or Western Isles, Na h-Eileanan Siar), NW Scotland, UK (Fig. 1). It typically dips 20-25° towards ESE on regional scale seismic imaging (Smythe et al., 1982) and cuts the Archean-Paleoproterozoic Lewisian complex (Fettes et al., 1981). The Lewisian in the Outer Hebrides predominantly consists of granulite and amphibolite facies banded felsic and pyroxene gneisses, together with subordinate units of meta-basic dykes, meta-anorthosite, meta-gabbro, and localised metasediments (Fettes et al., 1981).

Initiation of the OHFZ likely took place at ~1100 Ma, potentially related to Grenvillian tectonics (Butler et al., 1995; Imber et al., 2002). This is the maximum possible age for OHFZ movement, as it cuts late tectono-thermal structures dated to this time (Cliff and Rex, 1989) and consistently overprints Laxfordian age (~1700 Ma) pegmatites (Imber et al. 2002). The kinematic history of the OHFZ has been much debated since early work interpreted it to be dominantly thrust related (Coward, 1969; Francis and Sibson, 1973; Sibson, 1975). Many workers (Sibson, 1975; Butler et al., 1995; MacInnes et al., 2000; Osinski et al., 2001; Imber et al., 2002) agree that initial movement consisted of ductile top-to-NW thrusting, followed by later, shallower top-to-NW brittle thrusting during the Caledonian Orogeny. Later post-thrusting movement included spatially heterogeneous components of sinistral strike-slip (Butler et al., 1995; Imber et al., 2002) or a mix of sinistral and dextral strike-slip (MacInnes et al., 2000), followed by extension (White and Glasser, 1987; Butler et al., 1995; MacInnes et al., 2000; Imber et al., 2001; Osinski et al., 2001). The contribution of some extensional movement during the main brittle thrusting phase is disputed (White and Glasser, 1987; Imber et al., 2001; Osinski et al., 2001), as is the pervasiveness of late sinistral strike slip, leading to suggestions of a heterogeneous kinematic history along different fault segments (Butler et al., 1995; MacInnes et al., 2000; Osinski et al., 2001).

Within this evolving kinematic history, the type and sequence of fault rocks observed also varies between different segments of the OHFZ (Table 1). Amphibolite-facies mylonites relating to early

ductile initiation extend to thicknesses of 600 m in the north of the onshore OHFZ (Fig. 1), across the islands of Lewis and Sgalpaigh (Scalpay) (Butler et al., 1995). Further to the south, however, mylonites are only seen highly localised onto individual fault planes (Osinski et al., 2001). Brittle fault planes postdating these early ductile shear zones are widespread along the western extent of the main fault zone (shown as the fault trace in Fig. 1), incorporating pseudotachylyte and cataclasite (Sibson 1977; Butler et al., 1995; Imber et al., 1997). Fluid influx triggering greenschist-facies alteration and phyllonitisation occurred along the east of the fault zone, and it is these phyllonites and other low-temperature mylonites that record much of the late- to post-Caledonian strike slip and extensional phases (Butler et al., 1995; Osinski et al., 2001; Szulc et al., 2008). This fluid-rock interaction was not ubiquitous across the fault zone, resulting in lenses of phyllonite within retrogressed gneisses and locally preserving unaltered segments along the fault zone that appear to have escaped fluid influx altogether (Sibson, 1980; MacInnes et al., 2000). $^{40}Ar/^{39}Ar$ dating of OHFZ pseudotachylytes has generated Caledonian ages of 430 ± 6 Ma (Kelley et al., 1994), whilst others have yielded ages of 1900 Ma, ~1200 Ma and 700 Ma (Sherlock et al., 2009). Alternative causes for some or all of the Outer Hebrides pseudotachylytes have therefore been suggested as: a) early pseudotachylyte generation coeval with ductile thrusting on the OHFZ, observed so far only in the northern extent of the OHFZ (Sibson 1980; White 1996); b) distal seismicity as a response to tectonic regimes such as the Knoydartian orogeny - which may have also triggered pre-Caledonian initiation of the mainland Moine Thrust (Sherlock et al. 2009; Krabbendam et al. 2017); or c) impact-generated pseudotachylyte relating to an impact recorded by the Stac Fada member of the Mesoproterozoic Stoer Group on the Scottish mainland (Amor et al. 2008; Sherlock et al. 2009; Reddy et al. 2015, Amor et al., 2019). However, many of the pseudotachylytes are spatially related to the OHFZ (Fig. 1) and no unambiguous evidence for impact-related processes has yet been observed from the Outer Hebrides.

Pseudotachylytes occur in the OHFZ with a range of morphologies, including linear fault and injection veins, networks of veins, pseudotachylyte-matrix breccias and linkages between paired

faults (Fig. 2). Such structures record the sometimes complex geometry of the individual ruptures that generated the pseudotachylytes (Rowe et al. 2018). Pseudotachylyte-bearing faults are scattered quite widely across the Outer Hebrides, including in regions where other major fault structures are not apparent – for example, the west coasts of Barra and South Uist (Fig. 1). The melt-origin of these pseudotachylytes is recognised from features such as quench-crystallisation morphologies (e.g. spherulites, microlites and dendritic crystals), concave embayments into survivor clasts within the pseudotachylyte, and from the preferential breakdown of low-melting point minerals such as biotite and amphibole (Fig. 2). The fine-grained crystalline matrix of these OHFZ pseudotachylytes is typically composed of oligoclase plagioclase, hornblende and some biotite, broadly reflecting the host rocks present along the generation plane (O'Callaghan & Osinski, 2019), whilst unmelted clasts of the host rock are dominated by quartz and plagioclase. Alteration assemblages within the pseudotachylyte veins, where seen, are commonly chlorite and epidote, more rarely with actinolite and albite.

Pseudotachylyte generation planes, including linear fault veins (Fig. 2a) as well as fault breccias with a melt-derived matrix (Fig. 2b), show a variety of orientations (Fig. 1). A cluster of faults dip moderately NE through east to SE, with the modal dip direction oriented between 070-080°. There is no systematic variation in fault orientation seen with respect to the spatial location of the faults observed along strike on the OHFZ as the main fault trace curves northwards from NNE-SSW to NW-SEE (Fig. 1). Very locally, some systematic changes in orientation do exist, for example on Grimsay where a series of small backthrusts form a cluster dipping west or NW (Fig. 1, 'Northern Uists' stereonet). In southeastern South Uist the faults tend to be dipping more towards the NE and NNE compared to Barra to the south, which has a spread of dip directions from SE round to NE. The main trace of the OHFZ is also more NNE-SSW in southeastern South Uist compared to NE-SW in Barra, but this correlation does not seem to be maintained across other regions of the OHFZ (Fig. 1).

Methods

Fieldwork for this study investigated several sites along and around the main segments of the OHFZ (Fig. 1). Field observations focussed on recording the geometry and orientation of pseudotachylyte-bearing faults and associated features, with the aim of interpreting the sense of displacement. Fault-derived pseudotachylytes do not typically record slickenlines or other direct evidence of slip direction; although 'brushlines' formed by the coseismic drag of fault wall asperities across pseudotachylyte melt have been observed at the host rock – pseudotachylyte interface (Ferré et al. 2016), this surface is rarely exposed due to the tendency for pseudotachylytes to weld to the fault plane (Mitchell et al. 2016). Instead, three different approaches were utilised: (1) recording offsets indicated by displaced marker structures across pseudotachylyte-bearing faults; (2) recording orientations of systematic injection veins considered to have formed due to dynamic off-fault tensile cracking under the coseismic rupture-tip stress field; and (3) recording the orientations of en-echelon arrays of injection veins.

Field and microstructural markers of displacement direction

Direct field observations of planar markers offset across a fault, for example mineral banding or veins (Fig. 3a-d), were used to record the apparent slip sense of each fault. In addition, fault dip direction was recorded in order to investigate any link between fault orientation and slip sense. For example, the pseudotachylyte-bearing fault in Fig. 3a is recorded with apparent extensional offset of an earlier pseudotachylyte vein across a SE-dipping fault. Similarly, microstructural indicators of slip sense visible in thin sections of pseudotachylyte fault veins included small-scale offset markers, aligned clasts in the pseudotachylyte vein, and asymmetrical shear structures in the margins judged to be contemporaneous with melting (Figs. 3e,f). These were combined with field observations where the fault vein orientation was known. Unfortunately, it was not possible to reconstruct full slip vectors from this dataset, due to the lack of multiple displaced markers or striation-style transport direction indicators (c.f. Yamada & Sakaguchi, 1995, Xu et al., 2009). The observed offsets (apparent displacements) for this dataset range from 0.010 – 0.410 m, consistent with a range of

0.003 – 1.670 m reported for OHFZ pseudotachylyte faults in previous studies (Sibson, 1975, Hirose & Shimamoto, 2005, Nielsen et al., 2010).

Application of dynamic off-fault tensile crack model for determination of slip direction

During coseismic rupture and frictional melting along a fault plane, injection of melt away from the fault to form secondary veins into the surrounding host rock may occur (Figs 4a-d). These injection veins may exploit pre-existing fractures if they are present, but can also form via dynamic coseismic fracturing (Di Toro et al., 2005; Griffith et al., 2009; Ngo et al., 2012). Known as dynamic off-fault tensile cracks (e.g. Ngo et al., 2012), they initiate during rupture of the fault within the dynamic tensile stress field around the rupture-tip, and hence systematically fracture a single fault wall as the rupture-tip passes (Griffith et al., 2009; Ngo et al., 2012). The clearest distinction in natural faults of these dynamic cracks from other fracture sets is seen when a series of parallel cracks develops on one side of the fault (Fig. 4e). Such features have been observed in the form of tensile injection veins along pseudotachylyte faults (Di Toro et al., 2005; Ngo et al., 2012). The magnitude of the angle between a tensile crack and the fault is controlled by many factors, including slip velocity, fault frictional strength, velocity weakening behaviour, confining pressure and Poisson's ratio (Ngo et al., 2012, Alneasan et al., 2020), but in all cases, the sense of slip is towards the acute intersection between the crack and the fault (Fig. 4f, Di Toro et al., 2005; Griffith et al., 2009; Ngo et al., 2012). The slip vector is oriented perpendicular to the line of intersection between the tensile injection vein with the fault plane (Fig. 4f). Identifying the orientation of this intersection therefore allows the seismic slip direction to be determined.

Pseudotachylyte fault planes in the OHFZ were included for analysis of slip directions from off-fault tensile cracks if they displayed multiple sub-parallel injection veins restricted to a single side of the fault plane (Fig. 4a-d). Faults with single injections were also included if there were no injections on the opposing wall and if adjacent parallel faults with similarly oriented injection veins were observed within 0.5 m perpendicular to the fault. Orientations of injection veins and fault veins were

recorded, and the acute angle between injection veins and the fault was identified to determine the sense of slip (Fig. 4f). Because the best exposed examples of these features are often in flat vertical (Fig. 4a-b) or horizontal (Fig. 4c-d) faces, measurement of the injection veins can sometimes carry greater uncertainty than the ~±1° typical of field measurements, depending on the smoothness of the exposure surface, the occurrence of fractures cutting across and exposing different faces, and the extent of differential weathering of the pseudotachylyte relative to the host rock. The uncertainty of measurement was considered in the context of sets of injection veins at any one locality; either the orientation of the most reliable injection vein, or alternatively an average of multiple injection veins where of equal certainty, was used to derive the trend of slip via the perpendicular to the intersection (Supplementary Table 2). Fault slip analysis to determine the probable stress field during slip was then undertaken using a combination of the derived slip trend and fault orientation data. During this process, fault plane solutions for each pseudotachylyte-bearing fault were calculated using a kinematic approach from the maximum axes of compression and extension (e.g. Marrett and Allmendinger, 1990).

Further dynamic fault slip inversion for palaeostress analysis was conducted to constrain the possible stress fields for seismicity recorded by these pseudotachylyte faults (e.g. Angelier 1994, Žalohar and Vrabec, 2007). Several methods for fault inversion exist, including various methods of separating heterogeneous fault slip observations generated by changing stress fields (e.g. Nemcok and Lisle, 1995; Shan and Fry, 2005; Sato and Yamaji, 2006). Here, the Gaussian method of Žalohar and Vrabec (2007), is chosen due to its relatively good ability to form stable stress tensor solutions with differing and/or small fault numbers in each stress tensor subset, or with error in the slip sense of the fault planes, and to distinguish between stress tensors with small angular differences (> 10°). Importantly, the method (automated in the freely available software "T-Tecto X5", http://www2.arnes.si/~jzaloh/t-tecto_homepage.html) demands mechanical compatibility of the fault planes and their slip directions in order to contribute to a stress tensor solution – each fault must satisfy Amontons' Law, $\mu < \tau/\sigma_n$, where μ is the friction coefficient, τ the shear stress and σ_n

the normal stress on the fault plane. The inversion returns the best-fit reduced stress tensor - the orientations of the principal stresses ($\sigma_1 \geq \sigma_2 \geq \sigma_3$) and the stress ratio defining the relative stress magnitudes ($\phi = [\sigma_2-\sigma_3]/[\sigma_1-\sigma_3]$).

The method handles heterogeneous fault slip populations (i.e. faults and their slip directions that relate to several varying stress fields) by applying a best-fit stress tensor to a population of compatible faults. The workflow is described in full in Žalohar and Vrabec (2007), but here we summarise the approach. Firstly, the analysis takes the bulk input fault slip data and applies an object function that assesses the mechanical compatibility for all faults over a range of possible stress tensor orientations; the maxima of this object function distribution is used to locate the stress tensor for this first stage. Faults that have angular misfits between their ideal slip direction (i.e. the direction of maximum shear stress as per the Wallace-Bott hypothesis; Bott, 1959, Wallace, 1951) less than the user-defined misfit threshold (α) are considered compatible with this stress tensor. The process restarts using only the faults determined to be incompatible with the first stress tensor. The next best-fit stress tensor is constrained and again the angular misfit threshold α can be set to determine which faults can be included as compatible with this stress tensor. At this stage, faults that were associated with the first stress tensor can also be included if they meet the angular misfit threshold for the second stress tensor, which reduces the chance of ambiguous faults being wrongly removed from the analysis at an early stage. The second stress tensor can be reanalysed including such faults. The process is repeated further until all faults are accounted for. Several parameters can be set to refine the angular dispersion and the mechanical compatibility – our choice of values for these are detailed in the Supporting Information.

The available observations of fault slip directions are limited in number (n=35). Consequentially, these results are considered in conjunction with other field observations presented in this study in order to minimise the possibility of artefacts in the stress tensors produced from the fault inversion (Orife and Lisle, 2006).

Application of en-echelon models to pseudotachylyte injection veins

A common pseudotachylyte vein morphology across the OHFZ and elsewhere (e.g. Sibson, 1975; Hoek, 1991, Clarke & Norman, 1993, Garde & Klausen, 2016) is an en-echelon segmented array (Fig. 5). As these en-echelon veins lack displacement along them, they are likely to be injection veins (Garde & Klausen, 2016). This lack of displacement along with the tensile mode of fracturing needs to be identified, because similar geometries are also seen in stepped pseudotachylyte-bearing fault segments (e.g. Campbell et al., 2019). Where a three-dimensional example can be seen (Fig. 5e), the en-echelon segments are observed to branch out from a single vein. Three-dimensional exposures of these veins have not been found in-situ, but an array in an uncommon vertical exposure face (Fig. 5d) shows segmentation occurring at the tip of an injection vein in the direction of injection propagation away from a fault vein. In many cases (Figs. 5a-c) segmentation of steeply dipping veins is observed on near-horizontal surfaces and the fault plane is not seen. The array of en-echelon injection segments is sometimes diffuse, which may represent multiple veins (Fig. 5b) but, where a more linear arrangement exists, the long axis of individual veins may be either oblique (Fig. 5a) or parallel (Fig. 5c) to the overall array trend. Vein tips curve in towards an approaching or overlapping adjacent vein segment (Figs. 5c,d) but there is no obvious macroscopic deformation of the adjacent rock between veins. The direction of step between adjacent segments is not necessarily constant within any array.

The characteristics of these segmented pseudotachylyte arrays are more typical of en-echelon fracture models (e.g. Pollard et al., 1982) than of sigmoidal vein arrays formed in shear zones (e.g. Beach, 1975; Lisle, 2013). During propagation of a tensile crack (Fig. 6a), en-echelon segmentation can be induced by the presence of a resolved shear stress on the

284 walls of the crack (Fig. 6b). For example, a change in the stress field encountered during
285 continued crack propagation can result in a growing fracture, perhaps initially aligned to a
286 local or transient principal stress, progressively segmenting and rotating its propagation
287 trajectory in order to alignment with a remote or background principal stress field, ideally
288 ending up perpendicular to the minimum compressive stress (Pollard et al., 1982).
289 Depending on the point of exposure of the observed en-echelon array relative to the
290 position along the entire crack, the en-echelon segments may not necessarily be visible at
291 their point of maximum realignment towards any such stress field (Fig. 6c, Nicholson and
292 Pollard, 1985) and the maximum realignment may not necessarily be perfectly
293 perpendicular to the bulk extension direction (e.g. McCoss, 1986). The curvature seen at the
294 en-echelon segment tips is related to the interaction of adjacent or overlapping dilatant
295 segments (Pollard et al., 1982; Olson and Pollard, 1991).

296 En-echelon fracture and dyke models (e.g. Pollard et al., 1982; Nicholson and Pollard, 1985;
297 Olson and Pollard, 1991) are applied here to pseudotachylyte injection veins (Fig. 6c). We
298 test whether analysis of principal stress orientations similar to those performed on en-
299 echelon fractures, dykes and veins (e.g. Pollard et al., 1982; Rickard and Rixon, 1983) can be
300 made on pseudotachylyte geometries. In this context, the injection vein is initially a tensile
301 fluid-filled crack at the point where it originates from the fault plane (Fig. 6c). This 'parent'
302 injection vein is oriented perpendicular to the minimum compressive stress of the rupture-
303 tip stress field, which is transiently parallel to the slip direction under the off-fault tensile
304 crack model previously discussed (Ngo et al., 2012). As the rupture tip continues to
305 propagate along the fault plane away from the initiation point of any given injection vein,
306 and combined with the increasing distance of the vein tip from the fault plane as it
307 propagates into the host rock, the influence of the transient rupture–tip stress field wanes.

Instead, a remote stress field becomes the dominant influence on the trajectory of the injection vein, encouraging segmentation at the propagating vein tip to facilitate progressive rotation of the injection vein trajectory (Figs. 6b-c). This far-field stress field may be the regional tectonic stress field, or some modification of it imposed by larger-scale active structures in the vicinity of the observed pseudotachylyte-fault. Where an en-echelon array of pseudotachylyte injection veins is observed in the field, the trend of the whole array corresponds to the initial trace of the parent injection vein when it branched from the fault plane. Conversely, the orientation of each individual segment indicates the magnitude of rotation of the injection vein propagation path (Fig. 6c). Here, the orientations of individual segments are compared with the orientation of the overall array, with results presented as trends normal to the strike of the array and of the segment. We use the assumption that these approximate the local and far-field minimum compressive stresses, respectively (Pollard et al., 1982).

Results

Field and microstructural observations of slip sense

Both normal and reverse apparent fault movements are indicated by field and microstructural indicators of slip sense observed along various pseudotachylyte faults, in addition to two sinistral strike slip faults (Fig. 7). Normal offsets are predominantly hosted on faults with dip directions between north and NW, or between south, SE and east (n = 15). In contrast, faults with a reverse component generally dip to the west, or towards the NE (n = 19). Too few faults with significant apparent strike-slip components were observed to draw any valid conclusions (Fig. 7).

Slip directions from secondary dynamic tensile veins

Slip trends calculated from dynamic tensile injection veins (Fig. 4) are indicated with fault slip solutions and palaeostress analysis stereonets in Fig. 8. Shallowly plunging slip vectors dominate, with clusters indicating NE-SW and NW-SE trends. Several faults within this dataset are NE-dipping (Fig. 8); such faults occur in many localities across the OHFZ and many show oblique reverse senses of movement with both dextral and sinistral components (Figs. 1, 8). SE- and NW- dipping faults are also common. In any given location, a variety of fault orientations occur, with differing slip kinematics. Palaeostress analysis suggests that at least three stress fields are needed to account for this variation. Firstly, where the maximum principal stress (σ_1) is broadly NE-SW and the minimum principal stress (σ_3) is close to vertical, outlining an overall compressional stress field; this accounts for approximately one third of the faults analysed (n=11), including several of the NE-dipping oblique (right-lateral) reverse faults (Fig. 8, green stereonet). A second stress field has σ_1 horizontal E-W and σ_3 horizontal N-S (n = 10), and σ_3 and σ_2 are of similar magnitude. NE-dipping faults are also active within this stress field, but with a mixture of dip-slip reverse and left-lateral movement (Fig. 8, blue stereonet). A third stress field is also strike-slip, with near-vertical σ_2, NE-SW σ_3 and NW-SE σ_1. σ_1 and σ_2 are proposed to be of similar magnitude, so that the effect of σ_3 may be dominant; faults with some extensional component are attributed to this stress field (n=7, orange stereonet, Fig. 8). Four more faults can be attributed to another strike-slip stress field where σ_1 is WNW-ESE and σ_2 is NNE-SSW (pink stereonet, Fig. 8). The stress ratio is similar to the strike-slip stress field with NE-SW σ_3. The fault attributed to this stress field are mostly oblique left-lateral extensional. A further five faults have large misfits to all of these palaeostress solutions and do not combine in enough numbers to suggest any further stress fields, and so remain unattributed (Fig. 8).

Stress fields from en-echelon injection veins

The orientation of en-echelon pseudotachylyte injection vein arrays are described by the trend of the perpendicular direction either to an individual en-echelon segment (the segment-normal), or to the overall vein array (the array-normal). Across the dataset, the

355 segment-normals have a dispersed range of orientations with no obvious modal trend (Fig.
356 9a). However, they often lie within the range NW-SE to N-S (Fig. 9a). The array-normals have
357 a modal NW-SE trend, but also show N-S and E-W opening directions (Fig. 9b).

358 Within any en-echelon array, the segment-normal typically deviates at some angle from the
359 array-normal (Figs. 6c, 9c). The segment-normal may be found either clockwise and anti-
360 clockwise from the array-normal in the OHFZ pseudotachylytes. These senses of deviation
361 from the azimuth of the array-normal to that of the segment-normal are not restricted to
362 any particular orientation range of the parent array, but for each sense there is a peak in the
363 magnitude of deviation at a given azimuth of the array-normal (Fig. 9c). Typically, the
364 segments have an azimuthal deviation of ≤ 20° from the parent array. For the clockwise sense,
365 the maximum deviation is ~ 80° and occurs where the array-normal is ESE-WNW. For the
366 anti-clockwise sense, the maximum magnitude of deviation is ~50° and occurs when the
367 array-normal is ENE-WSW. In any single locality along the OHFZ region, similarly oriented
368 en-echelon arrays may show opposite senses of azimuth deviation, and a variety of
369 orientations exist (Fig. 10).

370 **Discussion**

371 Traditionally, the OHFZ has been considered as part of the Caledonian collisional system, due largely
372 to the widespread development of thrust kinematics and the overall NNE-SSW strike and ESE dip-
373 direction of the entire fault zone (Fig. 1), subparallel to the Moine Thrust on the Scottish mainland
374 (Smythe et al., 1982; Streule et al., 2010). This idea influenced early names for the OHFZ, including
375 'Outer Isles Thrust' (e.g. Coward, 1969; Sibson, 1975). However, the orientation of different
376 segments of the OHFZ varies on the kilometre scale, with local strikes varying from N-S through to E-
377 W (Fig. 1). Orientations of small length scale pseudotachylyte-bearing fault planes in the OHFZ are
378 also varied, with a higher proportion of NE-dipping faults than the large-scale OHFZ fault trace might

379 suggest (Fig. 1). Pseudotachylyte-bearing faults, which record seismicity, include a spectrum of
380 normal, reverse and strike-slip movement. The balance between reverse and normal faulting in
381 particular has been much discussed in several studies of the OHFZ (e.g. White and Glasser, 1987;
382 Osinski et al., 2001) and there are now a number of studies which recognise evidence for late
383 Caledonian reactivation of the OHFZ with strike-slip and extensional kinematics (see Table 1).
384 Pseudotachylyte-bearing normal faults in the OHFZ are sometimes suggested to have locally
385 accommodated block movements during the major thrusting phase of the OHFZ (Butler, 1995).
386 However, in southern portions of the onshore OHFZ, particularly in South Uist and Barra, kinematic
387 evidence for extensional faulting is locally more widespread than reverse movement (White and
388 Glasser, 1987; Osinski et al., 2001; see Table 1) and pseudotachylyte–bearing normal faults have
389 been shown to form part of a distinct, relatively late phase of extension (MacInnes et al., 2000). The
390 current study extends the discussion over the relative importance of the varying kinematics of fault
391 slip, focussed mostly on the seismic behaviour recorded by the pseudotachylytes, but considers also
392 the overall heterogeneity and temporal evolution in deformation behaviour on a long-lived and
393 reactivated fault zone such as the OHFZ.

394 *Controls on fault orientation in the OHFZ*

395 Amongst the variation in orientations of individual pseudotachylyte-bearing fault segments is a
396 prominent NE-dipping set (Fig. 1). Slip direction analysis indicates that these NE-dipping faults
397 accommodate a range of fault movements ranging from both left- and right- lateral strike-slip
398 through to oblique dip-slip and some dominantly dip-slip reverse faults (Fig. 8). This significant
399 number of NE-dipping faults accommodating slip within the OHFZ system, in contrast to the
400 approximate ESE-dipping trend of the main OHFZ fault trace, might suggest some control by other
401 structures on the orientation of fault formation. This could include reactivation of pre-existing fault
402 planes, or involve fault initiation exploiting alternative localised weak structures such as foliation or

403 lithological boundaries within the country rock. We briefly evaluate the potential influence of such
404 structures here.

405 Considering the first option, appropriate candidates for widespread pre-existent fault systems are
406 difficult to pinpoint as both Laxfordian (e.g. South Harris Shear Zones) and post-Caledonian faults,
407 whilst also striking NW-SE, are invariably steeper than the NE dipping pseudotachylyte-bearing faults
408 (Fettes et al., 1992; MacInnes et al., 2000). Within the Lewisian Gneiss Complex that hosts the OHFZ,
409 the most pervasive structure that could potentially have been exploited for slip is the foliation,
410 generally formed by gneissic banding (Fettes and Mendum, 1987). The banding concentrates layers
411 of minerals such as biotite and amphibole, which are likely to be mechanically and frictionally
412 weaker relative to quartzo-feldspathic layers (Spray, 2010). Additionally, the lower melting
413 temperatures of biotite and amphibole (Spray, 2010) may bias the generation of pseudotachylyte
414 onto faults along biotite- or amphibole-rich layers. The foliation across the Outer Hebrides, excluding
415 any mylonitic or cataclastic fabrics associated with the OHFZ, was regionally folded during pre-OHFZ
416 Laxfordian deformation, but typically dips moderately to steeply NE or northwards (Fettes et al.,
417 1992), similar to the pseudotachylyte-bearing faults (Fig. 1). However, pseudotachylyte generation
418 planes are rarely truly parallel to the immediately adjacent foliation (Fig. 11), although brecciated
419 faults in particular often lie at a low angle to it. Thus, the foliation does not appear to be exploited
420 directly for fault initiation, which may indicate either a high angle between the foliation and the
421 maximum compressive stress, or a large confining pressure (Tien et al., 2006). There is some
422 indication, however, that strong foliation planes oriented between 15-75° from the maximum
423 principal stress may facilitate a preferred orientation of shear fractures towards the foliation fabric
424 (Donath, 1961, Tien et al., 2006). This may explain why so many of the faults lie at relatively low
425 angles to the surrounding foliation, despite the suggested changes in stress field (Fig 8.) varying the
426 orientation of σ_1.

If no exploitable pre-existing structures are available, new faults with more ideal orientations should instead form, responding to the variation in stress fields suggested by the fault slip analysis (Fig. 8). NE-dipping faults may have preferentially formed when σ_1 or σ_3 was oriented NE-SW, for example. In fact, the major fault structures of the OHFZ (as mapped in Fig. 1) are more likely to represent the reactivation of pre-existing and potentially misoriented structures (Imber et al., 2002) than the small, apparently single-slip faults that we consider here. One scenario could be that NE-SW compression featured as an early transpressional stress regime preceding Caledonian convergence (Fig. 12), and scattered seismicity reflected the lack of a large through-going fault zone (the OHFZ) at this stage.

Alternatively, it remains possible that some number of the pseudotachylyte faults may pre-date Caledonian movement on the main trace of the OHFZ, bearing in mind that some OHFZ pseudotachylytes can be related with good certainty to Caledonian movement (Sibson, 1977a, Kelley et al., 1994, MacInnes et al., 2000). Early pseudotachylyte, viscously deformed within mylonite sequences (Sibson, 1980, White, 1996), may relate to (or predate) the proposed early phase of generally ductile reverse movement along the OHFZ (Imber et al., 2002), and equivalent age faults may be preserved without a viscous overprint outside the main shear zone localities. However, this phase of early OHFZ compression is also thought to have been top-to-NW (Imber et al., 2002), so does not help account for the variation in pseudotachylyte orientations that we observe here. The age of earliest possible OHFZ movement is set at ~ 1.1 Ga (Imber et al., 2002), constrained by the cessation of activity on the South Harris Shear Zones (Cliff & Rex, 1989). Earlier brittle faulting unrelated to the OHFZ is another possible scenario (Fig. 12); on mainland west-coast Scotland, 1.55 Ga brittle faulting within in the Lewisian complex has been identified in the Canisp Shear Zone (Hardman, 2019) alongside 1.5 Ga faulting near the Loch Assynt Fault, both of which appear linked to a regional (Assyntian) strike-slip deformation event (Holdsworth et al., 2020). Later brittle faulting in the Gairloch Shear Zones relates to regional deformation at 0.98-1.12 Ga (Sherlock et al., 2008). 40Ar-39Ar dating studies of the OHFZ pseudotachylytes do not particularly corroborate with any of

453 these regional events, but have confirmed that some of the OHFZ pseudotachylytes are of
454 Caledonian age (Kelley et al., 1994) whilst some are likely older (Sherlock et al., 2009).

455 Although the OHFZ pseudotachylytes are typically inferred to result from tectonic faulting (Sibson,
456 1975, MacInnes et al., 2000, Osinski et al., 2001, O'Callaghan & Osinski, 2019), an alternative
457 explanation for some proportion of the widespread faulting across the Outer Hebrides is sometimes
458 suggested to be impact cratering (Sherlock et al., 2009). Although no clear field or microstructural
459 evidence for shock deformation has been found around the Outer Hebrides, there is mounting
460 evidence that the 1.18 Ga Stac Fada Member of the Stoer Group, which crops out on the west-coast
461 Scottish mainland, represents an ejecta deposit (Amor et al., 2008, Reddy et al., 2015). Transport
462 direction indicators have promoted the idea that the impact site would likely sit offshore in the
463 Minch Basin, between the mainland and the Outer Hebrides (Amor et al., 2019), and whilst this
464 interpretation is contested (Simms, 2020), alternative impact sites have proved difficult to reconcile
465 in terms of size and location (Simms and Ernstson, 2019). The proposed site lies ca. 40 km from
466 Stornoway in eastern Lewis (see Fig. 14 of Amor et al., 2019). However, the relative positions of the
467 Outer Hebrides and the Scottish mainland have been modified by significant fault movement since
468 the impact date; although the sense and magnitude of such movement is not well constrained, it
469 likely included significant (90 km) strike slip movement associated with the OHFZ and sub-Minch
470 Basin faults (Piper, 1992, Whitehouse and Bridgewater, 2001), placing great uncertainty on the
471 spatial association of the OHFZ pseudotachylytes with the proposed impact site. It also follows that it
472 is difficult to predict the probable character and orientation of any impact-related pseudotachylytes;
473 veins interpreted as shock features in the centre of the Vredefort Dome crater (South Africa) are
474 characterised by small displacements, steep dips and a relatively random orientation (Dressler &
475 Reimold, 2004), but more distal pseudotachylytes exposed in the Sudbury Crater (Canada) are
476 related to frictional slip processes during crater collapse and reflect the crater geometry, forming
477 large ring faults (Thompson & Spray, 1996). Evidence for shear movement associated with the OHFZ
478 pseudotachylyte faults demonstrated in the current study may imply that, if any of these

pseudotachylytes were related to an impact event, they more likely relate to crater-related faulting, although the geometries of brecciation and injection are comparable with those exposed in Vredefort (Garde & Klausen, 2016). Whilst is it possible that some of the OHFZ pseudotachylytes were generated during an impact cratering event and do not represent a tectonic stress-field, significant numbers of pseudotachylyte faults across the Outer Hebrides remain likely to be tectonic.

Slip directions and stress fields of ancient seismicity on the OHFZ: comparison of methods

Interpreting the stress field from en-echelon pseudotachylyte arrays: uncertainties

Observations of en-echelon pseudotachylyte injection veins often lack constraint on the causative fault plane orientation, restricting a complete analysis of the stress field. According to the en-echelon model proposed above, however, the rotation of injection vein propagation trajectories to form en-echelon veins should provide some indication of the minimum principal stress direction even when the fault plane itself is not observed. In this model, en-echelon pseudotachylyte vein segments form by rotation of their propagation trajectory away from the initial orientation at the base of the injection vein, as the influence of the coseismic rupture-tip stress field wanes and a far-field tectonic stress field becomes the dominant control on tensile opening. However, in practice, analysis of the opening direction of the segments does not reveal clear trends (Fig. 9a). This may be because the segments either did not achieve the ideal angle of rotation during their propagation, or are not currently exposed at the level of their maximum azimuthal deviation, in order to align with the true direction of the far-field minimum compressive stress, or alternatively there are some invalid assumptions in this model. The extent of azimuthal deviation will depend on the difference in orientation between the dynamic rupture-tip and far-field stress fields, the distance the en-echelon segments have propagated from their origin at the fault vein, and at what level the plane of observation is along the length of the injection vein. The abundance of steeply dipping en-echelon segments may indicate that, for many of these seismic events, the far-field minimum compressive stress was close to horizontal. This implies that extensional and/or strike-slip stress regimes are

504 represented by these en-echelon arrays, in keeping with other evidence presented here for sets of
505 extensional and strike-slip pseudotachylyte faults.

506 The greatest magnitude of azimuth deviation of the en-echelon segment trajectories from the
507 parent array should occur when the array opening direction exhibits the most misorientation with
508 respect to the minimum compressive stress direction. As the largest magnitudes of azimuth
509 deviation are recorded when the array opening direction is between 080° and 110° (Fig. 9c), the
510 direction of σ_3 could be close to N-S. Under this stress field, where the maximum horizontal principal
511 stress is consequentially approximately E-W, west- or easterly-dipping faults should show reverse
512 movement, NE- or SW-dipping faults should show some element of left-lateral strike slip and NW- or
513 SE-dipping faults, right lateral. Such configurations account for observations of left lateral strike-slip
514 on NE dipping faults (Fig. 8). However, E- and W-dipping normal faults are better explained by
515 rotating the minimum principal stress towards a more E-W trend. Thus, whilst the en-echelon data
516 may not precisely define the directions of all three principal stresses, they do indicate that more
517 than one stress field is necessary to explain the observed fault slip directions, in line with field
518 observations of cross-cutting en-echelon vein arrays (Fig. 5a).

519 *Interpreting the stress field from palaeostress analysis: uncertainties and sources of error*

520 The use of dynamic tensile injection veins to firstly reconstruct the orientation of slip and then to
521 subsequently use those slip directions in palaeostress inversion is a novel approach, but it involves
522 repeating stages of interpretation and analysis, potentially allowing the propagation of errors
523 through to the resulting stress tensors. However, whilst errors in the slip direction identification will
524 certainly lead to errors in the stress tensor orientation, these may only become significant when the
525 error in the slip direction is >10° (Žalohar & Vrebac, 2007).

526 Another source of uncertainty in the stress field interpretation is the relatively small dataset of fault
527 orientations and slip directions, which leads to some stress tensor solutions being based on smaller
528 than ideal fault populations (i.e. > 9, Orife & Lisle, 2006); also, the greater the number of stress

tensor solutions suggested, the more likely that each solution has a low number of faults attributed to it. In addition, the Gauss method used cannot distinguish stress tensors with < 10° difference in the orientation of principal stresses, although it has greater resolution than other palaeostress methods (Žalohar & Vrebac, 2007). This prompts us to avoid the use of overly narrow subsets (see Supplementary Information); however, the resulting risk is that a best-fit stress tensor is produced that is not a reflection of any real stress field, but an amalgamation of several similar solutions. We additionally disregard stress tensor solutions output by the palaeostress analysis based on fault numbers below that which should be mathematically stable (i.e. n = 4, Etchecopar et al., 1981). One palaeostress solution has n = 4 (pink stereonet, Fig. 8), and the weight we place on its interpretation is discussed below. If, as we suggest, the pseudotachylyte faults represent long-lived seismic activity throughout progressive changes to the stress field, a large number of stress tensors showing progressive long-term rotation of the principal stresses might be the most realistic approximation. Nevertheless, the method still highlights clearly that no single stress field can explain all of the fault slip data.

A further source of uncertainty are the input parameters defined during palaeostress analysis. We have tested the results for sensitivity to varying these parameters within a reasonable range of values (Supp. Fig. 1 and accompanying text). If we vary the dispersion of angular misfit between the ideal and real slip direction, or the threshold for mechanical compatibility (see Supp. Info), the main differences in the stress tensor solutions are that there may be another dominantly compressional field where σ_1 is NW-SE (i.e. a more typical 'Caledonian' shortening trend), or that the NE-SW σ_3 strike-slip stress field may be an extensional stress field. Otherwise, the results using various input parameters (Supp. Fig. 1) tend to be similar to those presented in Fig. 8.

The interpretation of palaeostress fields from fault slip inversion methods involves a number of general assumptions (e.g. Simón, 2018, and references therein): (i) that there can be no differential rotation between bodies of rock separated by faults; (ii) that there is no interaction between faults

554 or pre-existing anisotropy that controls the fault orientation and slip; (iii) that the volume of rock
555 considered is much larger than the length scale of the faults; and (iv) that the faults are much larger
556 than the scale of displacement. In the OHFZ, the pseudotachylyte-bearing faults studied are small,
557 typically less than ~10 m in length, and subsequently displacements are also small. Any slip-
558 facilitated rotation across these faults is therefore expected to be minimal. Rotation of larger-scale
559 fault blocks is worth greater consideration because the observations are taken from a large area that
560 is subdivided by later faulting (Fettes et al., 1981). However, these late faults tend to be subvertical
561 strike-slip faults (MacInnes et al., 2000) and are therefore unlikely to have induced significant
562 differential rotation across the Outer Hebrides. The entire Outer Hebrides block, including the OHFZ,
563 was likely uplifted and rotated as a footwall block during the Mesozoic initiation of the Minch Fault,
564 and may have been rotated about a subhorizontal NE-SW axis by up to 15° towards the WNW
565 (Roberts and Holdsworth, 1999). Such a rotation would have had the effect of steepening ESE- and
566 easterly-dipping faults without inducing significant change to the principal stress directions
567 calculated from present day fault orientations. Considering other assumptions of the fault slip
568 analysis, interaction between faults in the OHFZ is difficult to interpret and, as previously discussed,
569 fault orientation may have been influenced by the foliation. However, the volume scaling between
570 overall volume, fault length and displacement is generally considered a valid assumption in this
571 study.

572 *Comparison of slip direction and stress field results*

573 Collating the results from each of the approaches used in this study (i.e. offset markers, en-echelon
574 vein arrays and dynamic tensile injection veins) indicates that two slip directions, NW-SE (varying to
575 WNW-ESE) and NE-SW (varying to NNE-SSW), appear to dominate. The stress field orientations
576 necessary for these fault populations are most readily interpreted from palaeostress analysis on the
577 dynamic injection vein observations, but these must corroborate with more tentative interpretations
578 from the other approaches. Because datasets for each method of analysis are relatively small, there

579 is potential for results to be skewed by a small, unrepresentative input dataset. However, by
580 comparing the independent datasets for each method, any such problem should be recognised. Both
581 the en-echelon veins and the off-fault tensile injection vein analyses suggest that σ_3 may have varied
582 in orientation between east-west and north-south (or NE-SW) at different stages. This orientation
583 for σ_3 corresponds broadly to the two strike-slip stress fields suggested by fault slip analysis,
584 although σ_3 is not implied there to be exactly E-W (Fig. 8).

585 Another stress field suggested by palaeostress analysis is compressional, where σ_3 is sub-vertical and
586 σ_1 is NE-SW (Fig. 8). This stress field is seemingly not recorded in the en-echelon dataset, possibly
587 because the majority of observed en-echelon veins are steeply dipping. A sub-vertical σ_3 would
588 ideally encourage injection veins to shallow as they propagated away from the generating fault, and
589 this geometry may be less likely to be visible on the frequently near-horizontal exposures. The
590 compressional field is considered unlikely to be an artefact for several reasons: firstly, due to the
591 relatively large number of faults that are included in this field (11 out of a total 30 observations, Fig.
592 8), and secondly, because the reverse NW-SE slip direction frequently recorded by both the field
593 offset data (Fig. 7) and the tensile injection vein analysis can be partly attributed to this
594 compressional field (Fig. 8). Compressional faulting in general is well documented across non-
595 pseudotachylyte-bearing faults and fault rocks in the OHFZ, although the inferred direction of
596 compression tends to be NW-SE, parallel to the most typically observed slip directions (e.g. Sibson
597 1977b, Fettes et al. 1992, Butler et al., 1995; MacInnes et al., 2000; Osinski et al., 2001; Imber et al.,
598 2002, Ferré et al., 2016). Some combinations of the palaeostress analysis input parameters do
599 suggest a stress field with NW-SE directed compression (Supp. Fig. 1), but always in addition to a NE-
600 SW directed compressional field. One of the strike-slip stress fields (with E-W σ_1) also accounts for
601 NW-SE slip directions on faults with some reverse component (blue stereonet, Fig. 8). We do
602 therefore do not rule out any period of NW-SE directed compression, but we interpret our results to
603 suggest that a phase of NE-SW compression also occurred.

The NE-SW σ_3 strike-slip stress field (orange stereonet, Fig. 8) is derived from a smaller number of faults (7 out of a total 30) showing mainly normal-component movement of varying obliquity (Fig. 8), with the fault planes dipping predominantly to the west and to the NE and slip directions to the north, ENE and SW. Most faults with a component of normal movement are incorporated in this field from the tensile injection vein dataset. In contrast, the offset marker data mostly show faults with apparent normal slip to dip towards the east, SE and to some extent NW to northwards (Fig. 7). It may be that a greater variety of normal-component faults exist than are included in the palaeostress analysis. This NE-SW σ_3 stress field also lacks the optimum threshold number of faults for a stable analysis (9, Orife & Lisle, 2006), as does an additional stress field with NNE-SSW σ_1 (pink stereonet, Fig. 8) that also incorporates extensional-component faults (though these are dominantly strike-slip), in this case with NNW-SSE slip vectors. Although proposed as a palaeostress solution, it has attributed to it a very small number of faults (n = 4, Fig. 8). For this reason we do not place any great weight on this additional stress field, except to consider that the similarity of the stress ratio and the simple rotation of σ_3 and σ_1 between this stress field and the strike-slip field where σ_3 is NE-SW may imply that both are related and provide approximations of some progressive rotation. Despite the small fault numbers attributed to each of these stress fields in the fault slip analysis, faults with a normal component are not rare in the offset marker database (Fig. 7) and, in the west- and NE- dipping orientations suggested there, are unlikely to be mechanically attributable to the compressional and E-W σ_1 strike-slip stress fields also suggested by the palaeostress analysis. Hence, we do expect that the majority of extensional pseudotachylyte-bearing faults relate to a separate stress field, even though the orientation of that stress tensor remains uncertain.

The stress field for each pseudotachylyte fault may be subject to local spatial or temporal variations, which means that the 'far-field stress' from the en-echelon analysis may not be equivalent to the regional tectonic-scale stress. This effect introduces some uncertainty into the stress tensor results from palaeostress analysis as well as some misfit of fault slip orientations in the population associated with each resulting tensor. These stress variations may be spatial, relating to changes in

orientation of the major fault structures of the OHFZ. Alternatively, there may be an additional temporal aspect, either spanning long-term changes as the fault network geometry evolves over time (Moir et al., 2010), or where local stresses change within seismic timescales, where the stress field is transiently perturbed by seismic activity on nearby fault segments (e.g. Das & Scholz, 1981, Nüchter & Ellis, 2011, Dempsey et al., 2014), including potentially within a single, complex rupture (e.g. as during the 2016 MW 7.8 Kaikoura earthquake., Hollingsworth et al., 2017). There is no obvious pattern of systematic changes in the stress field between different localities in the OHFZ (Figs. 8 & 10) that would indicate a purely spatial influence. Any localised temporal stress variation is also difficult to resolve from the general heterogeneity and the regional-scale change of stress field that we infer here. However, whilst it does not add enough uncertainty to alter our interpretation of ongoing seismicity during major changes to the stress field around the OHFZ, the potential for these local variations should be borne in mind when comparing individual faults, especially those situated significant distances apart.

There are few existing data on slip directions for seismic, pseudotachylyte-generating faults in the OHFZ with which to compare the slip direction results derived in this contribution. This is primarily due to the lack of markers from which to easily collect field observations. A recent anisotropy of magnetic susceptibility (AMS) analysis on an OHFZ pseudotachylyte sample from western South Uist interpreted top-to-the-WSW movement on an ENE dipping fault plane (Ferré et al., 2016), which fits with the data collected here for the subset of NE- and E- dipping reverse faults which would have had top-to-SW movement if predominantly dip-slip (Fig. 8). The lack of existing data means that the analyses presented here, whilst still limited in number by the availability of the appropriate field observations, remain a valuable attempt to further constrain both the seismic kinematics of the OHFZ and the general evolution of seismicity as long-lived fault zones reactivate under different kinematic conditions.

Synthesis of stress fields for seismicity with the history of the OHFZ

655 The framework of movement on the OHFZ within which to understand the context and potential
656 timing of the results presented above has been previously established to some extent in the existing
657 literature (Table 1). Whilst these new results for the kinematics of seismicity on the OHFZ fit into this
658 framework, they also introduce additional evidence - primarily the recognition of a period where the
659 maximum compressional stress was more NE-SW than NW-SE. In addition, the identification of
660 dominantly extensional seismicity (producing pseudotachylyte) in a distinct kinematic phase of OHFZ
661 activity increases the spatial extent of similar observations previously constrained to north Barra by
662 MacInnes et al. (2002).

663 A phase of brittle reverse faulting in the OHFZ, dominantly top-to-NW, is usually attributed to
664 Caledonian thrusting (e.g. Sibson, 1975, and others – see Table 1) and remains the major contender
665 to explain NW-SE reverse movement on these ancient seismic faults. It should be noted, however,
666 that an earlier top-to-NW kinematic phase around 1.1 Ga is also proposed for initiation of the OHFZ
667 (Imber et al., 2002). Although this phase is assumed to involve deeper crustal viscous deformation,
668 the presence of mylonitised pseudotachylytes in parts of the OHFZ (Sibson, 1980; White, 1996) and
669 older ^{40}Ar-^{39}Ar dates from OHFZ pseudotachylytes (Sherlock et al., 2009) mean that a wider record of
670 pre-Caledonian top-to-NW seismicity cannot be entirely ruled out. However, pseudotachylyte-
671 bearing OHFZ faults in this study do not explicitly indicate that top-to-NW directed thrusting was the
672 dominant component of seismic activity on the OHFZ. Whilst a NW-SE slip trend is apparent (Figs. 7,
673 8, 9a), many of these faults are somewhat extensional, where the slip sense is known. Rather, the
674 pseudotachylyte data suggest NE-SW compression, which is not only more difficult to match to
675 known NW-SE or E-W shortening directions of mainland thrusting but also to other OHFZ reverse
676 faults (Coward, 1969, 1983; Sibson, 1977b). However, the identified NE-SW trend of σ_1 in this
677 configuration could induce left lateral strike slip on SE- dipping faults, a kinematic phase observed in
678 the OHFZ particularly on phyllonite shear zones (Butler et al., 1995; Imber et al., 1997).

679 In contrast, the strike-slip stress field predicted by the palaeostress analysis where σ_1 is E-W has
680 induced right lateral slip on SE-dipping faults (Fig. 8). The left-lateral strike slip reported by Butler et
681 al. (1995) has been previously noted to be absent along some segments of the OHFZ, even where
682 phyllonites are still present, especially towards the south of the fault zone in South Uist (Osinski et
683 al., 2001) and Barra (MacInnes et al., 2000). Late Caledonian right-lateral strike slip faults with
684 pseudotachylyte are reported by MacInnes et al. (2000) in Barra, alongside left-lateral equivalents.
685 Our dataset also reports a mix of left- and right-lateral strike slip faults from several locations across
686 the OHFZ, including western Barra, western South Uist, SE Lewis and west Lewis; some of these
687 faults are attributed to the NE-SW compressional field and some of which are attributed to the E-W
688 σ_1 strike-slip stress field (Fig. 8). It would be, therefore, an over-simplification to attribute all strike-
689 slip faulting to the same late Caledonian strike slip phase as that recognised in the phyllonites (Butler
690 et al., 1995). Our new data therefore add to the growing consensus that deformation mechanisms
691 and kinematics along the OHFZ were highly variable across different segments (Butler et al., 1995,
692 MacInnes et al., 2000, Osinski et al., 2001).

693 An extension-dominated regime of fault movement and seismicity is implied in our results (Fig. 8)
694 and has been previously recognised across the OHFZ based on other field evidence, overprinting late
695 Caledonian strike-slip deformation (Butler et al., 1995, MacInnes et al., 2000). A late Caledonian
696 extensional phase is often included in discussion of the OHFZ's evolution, distinct to the later
697 Mesozoic extensional phase that formed the North Minch and Sea of Hebrides basins to the east
698 (Butler et al., 1995, MacInnes et al., 2000, Imber et al., 2001, Osinski et al., 2001, Szulc et al., 2008).
699 The extensional faulting is associated with an overall strike-slip stress field in our palaeostress
700 analysis, although with a similar magnitude of σ_2 and σ_1 , so that σ_3 seems dominant (and indeed
701 some combinations of input parameters suggest that this could be a true extensional stress field,
702 Supp. Fig. 1). The extensional faults observed in this study are scattered around the OHFZ (Fig. 8),
703 extending reports of significant Caledonian brittle normal faulting, including pseudotachylyte-
704 bearing faults, from previous observations in North Uist, South Uist and Barra (White and Glasser,

1987, MacInnes et al., 2000, Osinski et al., 2001). As with all small faults, it is often difficult to date, even relatively, the movement(s) that they represent. Additionally, we do not have a sufficient number of observations of cross-cutting relationships on pseudotachylyte-bearing faults to meaningfully support our arguments. However, where these are found, evidence from cross-cutting pseudotachylytes reported in this study do illustrate that normal faulting (Figs. 3a-b) and/or a NE-SW minimum principal stress (Fig. 5a) were in some instances the later (or last) seismic event.

Our results also confirm that extensional seismic faulting on the OHFZ was largely a response to a separate kinematic regime, rather than localised accommodation or partitioning of deformation during an overall compression (MacInnes et al., 2000, Osinski et al., 2001). Although the trend of σ_3 is not confidently constrained, this variation in movement supports the observations of Osinski et al. (2001) on phyllonites and brittle normal faults along the North and South Uist sections of the OHFZ.

Overall, the slip directions and stress fields implied by our new dataset of pseudotachylyte-bearing, ancient seismic faults along the OHFZ fit with other field observations on brittle faults, pseudotachylyte-bearing faults and ductile shear zones (Table 1). They could support the proposed model of progressive transition from orogenic compression through oblique convergence to late extension-dominated tectonics to explain the kinematics of various segments of the OHFZ, possibly through the Caledonian orogenic event (MacInnes, 2000, Imber, 2001, Osinski, 2001). The relative scatter of pseudotachylyte-bearing faults illustrated here indicate that the stress fields inferred from fault slip analysis could be the result of a progressively rotating tectonic stress field (Lacombe, 2012) during which seismic behaviour was episodically active along several sections of the OHFZ. However, it should be noted that all the observations here, and in other field studies recording the kinematics of brittle faulting on the OHFZ (e.g. MacInnes et al., 2000, Osinski et al., 2001) consider dispersed faults <10 m in exposed length. This is in contrast to the major fault segments, for example the 'crush zone' localities occurring in places such as Bealach an Easain, South Uist (Fig. 8) where faulting, fragmentation and chaotic cataclasite and pseudotachylyte networks makes clear

730 interpretations difficult, despite these being clearly important fault segments with significant fault
731 displacement.

732 *Implications for long-lived reactivated crustal faults*

733 Continuous episodic seismicity through several kinematic phases of an orogen indicates that parts of
734 a fault zone must remain strong and frictional, even if aseismic creep along weaker fault segments
735 apparently accommodates some component of the far-field stress. Recognising this behaviour, and
736 understanding where seismicity may nucleate, is important in the assessment of the seismic hazard
737 along active faults, even where the likely magnitude of seismicity is small. Sections of the OHFZ have
738 been used to illustrate how major reactivated fault zones weaken over time due to transformations
739 to phyllosilicate-rich fault rocks and subsequent changes in deformation mechanisms (Imber et al.,
740 1997). Comparisons have been made with processes occurring at depth along active fault zones such
741 as the San Andreas (e.g. Holdsworth et al., 2011) and the Karakoram (Wallis et al., 2015). However, a
742 growing body of evidence (including the current study) suggests that the OHFZ was highly
743 heterogeneous along strike in terms of fault rock development, deformation mechanisms and
744 accordingly fault strength for potentially much of its active history (MacInnes et al., 2000, Osinski et
745 al., 2001). This is consistent with the identification in other exhumed fault zones of variable strength
746 and structure evolution along different fault segments (Lawther et al., 2016), and multiple
747 deformation mechanisms (Kirkpatrick & Shipton, 2009) including the identification of a coeval
748 combination of periodic seismicity contemporaneous with ongoing aseismic creep along crustal scale
749 faults at seismogenic depths (Edwards & Ratschbacher, 2005, Faulkner et al., 2008). Such complexity
750 should therefore also be expected in present-day active fault zones. Understanding the fault
751 structure and strength profile is hence important in assessing where earthquakes could nucleate.

752 The OHFZ provides a useful addition to the growing record of exhumed faults exhibiting mixed
753 seismic slip and aseismic creep. In particular, the spatial scatter of seismicity away from the
754 phyllonite belts provides an alternative geometrical model to that of interconnected networks of

weak aseismic material surrounding isolated seismic blocks (e.g. Faulkner et al., 2003, Fagereng & Sibson, 2010). The new dataset suggests that seismic faults were present along several sections of the fault zone during the strike-slip and extensional phases of the OHFZ, in regions both with and without major phyllonite-related fault weakening (Fig. 8). In the first case, dispersed seismicity feasibly represents episodic strain accommodation in the wall rock that cannot be localised into the weak deforming phyllonite fault zone, and perhaps maintains some strain compatibility between the weak phyllonite and the relatively strong wall rock, as is inferred adjacent to weak creeping faults elsewhere (e.g. Faulkner et al., 2003). In the case that the seismicity occurs along a fault segment lacking phyllonitic development (e.g. as detailed in MacInnes et al. 2000), the maximum rupture length is the size of the strong fault segment, whereas in the case that the seismicity occurs in strong wall rock near to phyllonite segments, the distributed faulting may be more fully characterised by small length scale ruptures with low moment magnitudes.

The general character of scattered seismicity across the OHFZ (Fig. 12), including several localities not generally considered to lie within the main fault zone (Figs. 1, 8), argues for a lack of localisation in basement faulting. Whilst the OHFZ is typically mapped as a single major fault trace, most continental thrust faults involve several major fault strands linked by smaller, but still potentially seismogenic, fault strands (e.g. Lin et al. 2011; Cheloni et al. 2016). It is likely that several small basins offshore west of the Outer Hebrides were formed by inversion of reverse faults parallel to, and probably coeval with, the main onshore trace of the OHFZ (Hitchen et al. 1995), and so the scattered pseudotachylytes may well be linked to a much wider fault system, of which the OHFZ is merely an onshore, exposed part. In addition, generation of pseudotachylyte along a fault tends to weld the fault plane and preclude further reactivation of that fault patch under brittle upper crustal conditions (Mitchell et al., 2016), encouraging delocalisation of seismicity. This relative strength of the fault and the host rock has been suggested by others (Faulkner et al., 2008, Lawther et al., 2016) to be a major control on whether faulting at seismogenic depths becomes localised or remains dispersed. The OHFZ supports this model as the pseudotachylyte-bearing faults generally do not

indicate reworking of earlier pseudotachylytes from the same fault plane; rather, they display clusters of adjacent pseudotachylyte faults, suggesting that forming a new slip plane was easier than re-rupturing an existing pseudotachylyte-bearing fault. This model is not only limited to fault zones where pseudotachylytes are present, but is also applicable where mineralisation strengthens the fault (Lawther et al., 2016), or where weak fault rocks form in the fault zone but the host rock is of a similar strength (Faulkner et al., 2008), or where a series of scattered precursor structures (typically joints in crystalline basement) are weaker than the faults that exploit them (Faulkner et al., 2008). Where this strength ratio is controlled by permeability, fluid flow and type of mineralisation, it may change over time in a series of strength cycles causing a set of fault segments to experience variable drive to become active or to switch off (Lawther et al., 2016). However, in the case of pseudotachylyte fault welding, the drive to remain dispersed is likely to continue even in relatively mature fault zones (c.f. Ben-Zion & Sammis, 2003).

Some of the small faults hosting pseudotachylyte away from the main fault zone could also represent aftershocks that might have been encouraged to nucleate in off-fault areas in response to, for example, Coulomb stress changes driven by seismicity on the main fault (Das and Scholz, 1981). Such a suite of aftershocks may record a range of slip modes and stress fields that are not representative of the mainshock (Schulz & Evans, 2000; Dempsey et al., 2014; Cheng et al., 2018) and could provide an alternative explanation for the variable nature of fault kinematics in the OHFZ. Nevertheless, the seismic hazard of aftershocks may still be high (e.g. Gorkha earthquake, May 2015, Avouac et al., 2015). Thus, the inclusion and understanding of off-fault seismicity in all forms of fault-zone study is crucial to understanding the stress field and energy release of large-scale fault zones (Ross et al., 2017; Cooke and Beyer, 2018).

Conclusions

Ancient seismic faults in the exhumed OHFZ, represented by pseudotachylyte-bearing fault planes, record a range of slip directions for the fault zone, suggesting that seismicity involved the full

spectrum of reverse, normal and strike-slip fault movements. In part, this relates to variation in fault plane orientations, which diverge from the average ESE-dip direction of the large-scale OHFZ. Whilst the typical Caledonian thrusting traditionally attributed to the OHFZ pseudotachylytes has a NW-SE slip trend, the pseudotachylyte faults considered here suggest an additional NE-SW slip trend and σ_1 direction for a compressional stress field. The pseudotachylytes record that seismicity was related to multiple kinematic regimes, and could potentially represent the continuation of seismicity through progressively oblique Caledonian convergence, strike-slip and late Caledonian extension. Even if some of the pseudotachylytes were generated outside of the Caledonian, ongoing seismicity over multiple tectonic regimes implies that segments of the major faults may remain frictionally strong through episodes of repeated activation, despite the evolution to weak deformation mechanisms along some portions of the fault.

Acknowledgements

LC gratefully acknowledges funding from NERC (Studentship 1228272) and a National Museums Scotland CASE award that facilitated this work. Harri Wyn Williams is thanked for help with sample preparation and Richard Walshaw for SEM support at the Leeds Electron Microscopy and Spectroscopy Centre. T-TECTO software was funded by Quantectum AG, and by the Slovenian Research Agency (ARRS), the Republic of Slovenia, research project 1555-007-P1-0195. Zoe Shipton and an anonymous reviewer are thanked for their comments on this manuscript, which has greatly improved the work.

References

Alneasan, M., Behnia, M. & Bagherpour, R. 2020. The effect of Poisson's ratio on the creation of tensile branches around dynamic faults. Journal of Structural Geology, 131, 103950, https://doi.org/https://doi.org/10.1016/j.jsg.2019.103950.

831 Amor, K., Hesselbo, S.P., Porcelli, D., Thackrey, S. & Parnell, J. 2008. A Precambrian proximal ejecta
832 blanket from Scotland. Geology, 36, 303–306, https://doi.org/10.1130/g24454a.1.

833 Amor, K., Hesselbo, S.P., et al. 2019. The Mesoproterozoic Stac Fada proximal ejecta
834 blanket, NW Scotland: constraints on crater location from field observations,
835 anisotropy of magnetic susceptibility, petrography and geochemistry. Journal of the
836 Geological Society, 176, 830 LP – 846, https://doi.org/10.1144/jgs2018-093.

837 Angelier, J. 1994. Fault slip analysis and paleostress reconstruction. In: Hancock, P. (ed.) Continental
838 Deformation. New York, Pergamon, 53–100.

839 Avouac, J.-P., Meng, L., Wei, S., Wang, T., Ampuero, J.-P., 2015. Lower edge of locked Main
840 Himalayan Thrust unzipped by the 2015 Gorkha earthquake. Nature Geoscience 8, 708.

841 Beach, A., 1975. The geometry of en-echelon vein arrays. Tectonophysics 28, 245–263.
842 https://doi.org/https://doi.org/10.1016/0040-1951(75)90040-2

843 Behr, W.M., Platt, J.P., 2014. Brittle faults are weak, yet the ductile middle crust is strong:
844 Implications for lithospheric mechanics. Geophysical Research Letters 41, 2014GL061349.
845 https://doi.org/10.1002/2014gl061349

846 Ben-Zion, Y. & Sammis, C.G. 2003. Characterization of Fault Zones. Pure and Applied Geophysics,
847 160, 677–715, https://doi.org/10.1007/PL00012554.

848 Bott, M.H.P., 1959. The Mechanics of Oblique Slip Faulting. Geological Magazine 96, 109–117.
849 https://doi.org/DOI: 10.1017/S0016756800059987

850 Brewer, J.A., Smythe, D.K., 1986. Deep structure of the foreland to the Caledonian Orogen, NW
851 Scotland: Results of the Birps Winch Profile. Tectonics 5, 171–194.
852 https://doi.org/10.1029/TC005i002p00171

853 Butler, C.A., 1995. Basement fault reactivation: The kinematic evolution of the Outer Hebrides Fault
854 Zone, Scotland. Durham University.

855 Butler, C.A., Holdsworth, R.E., Strachan, R.A., 1995. Evidence for Caledonian sinistral strike-slip
856 motion and associated fault zone weakening, Outer Hebrides Fault Zone, NW Scotland. Journal
857 of the Geological Society 152, 743–746. https://doi.org/10.1144/gsjgs.152.5.0743

858 Campbell, L.R., Phillips, R.J., Walcott, R.C. & Lloyd, G.E. 2019. Rupture geometries in anisotropic
859 amphibolite recorded by pseudotachylytes in the Gairloch Shear Zone, NW Scotland. Scottish
860 Journal of Geology, 55, sjg2019-003, https://doi.org/10.1144/sjg2019-003.

861 Cheloni, D., Giuliani, R., et al. 2016. New insights into fault activation and stress transfer between en-
862 echelon thrusts: The 2012 Emilia, Northern Italy, earthquake sequence. Journal of Geophysical
863 Research: Solid Earth, 121, 4742–4766, https://doi.org/10.1002/2016JB012823.

864 Cheng, Y., Ross, Z.E., Ben-Zion, Y., 2018. Diverse Volumetric Faulting Patterns in the San Jacinto Fault
865 Zone. Journal of Geophysical Research: Solid Earth 123, 5068–5081.
866 https://doi.org/10.1029/2017JB015408

867 Clarke, G.L. & Norman, A.R. 1993. Generation of pseudotachylite under granulite facies
868 conditions, and its preservation during cooling. Journal of Metamorphic Geology, 11,
869 319–335, https://doi.org/10.1111/j.1525-1314.1993.tb00151.x.

870 Clemente, C.S., Amorós, E.B., Crespo, M.G., 2007. Dike intrusion under shear stress: Effects on
871 magnetic and vesicle fabrics in dikes from rift zones of Tenerife (Canary Islands). Journal of
872 Structural Geology 29, 1931–1942. https://doi.org/http://dx.doi.org/10.1016/j.jsg.2007.08.005

873 Cliff, R.A., Rex, D.C., 1989. Short Paper: Evidence for a 'Grenville' event in the Lewisian of the
874 northern Outer Hebrides. Journal of the Geological Society 146, 921–924.
875 https://doi.org/10.1144/gsjgs.146.6.0921

876 Collettini, C., Niemeijer, A., Viti, C., Marone, C., 2009. Fault zone fabric and fault weakness. Nature
877 462, 907–910.

878 Cooke, M.L., Beyer, J.L., 2018. Off-Fault Focal Mechanisms Not Representative of Interseismic Fault
879 Loading Suggest Deep Creep on the Northern San Jacinto Fault. Geophysical Research Letters
880 45, 8976–8984. https://doi.org/10.1029/2018GL078932

881 Cowan, D.S., 1999. Do faults preserve a record of seismic slip? A field geologist's opinion. Journal of
882 Structural Geology 21, 995–1001. https://doi.org/10.1016/S0191-8141(99)00046-2

883 Coward, M.P., 1983. The thrust and shear zones of the Moine thrust zone and the NW Scottish
884 Caledonides. Journal of the Geological Society 140, 795–811.
885 https://doi.org/10.1144/gsjgs.140.5.0795

886 Coward, M.P., 1969. The structural and metamorphic geology of South Uist, Outer Hebrides.
887 University of London.

888 Dalguer, L.A., Irikura, K., Riera, J.D., 2003. Simulation of tensile crack generation by three-
889 dimensional dynamic shear rupture propagation during an earthquake. Journal of Geophysical
890 Research: Solid Earth 108, 2144. https://doi.org/10.1029/2001JB001738

891 Das, S., Scholz, C.H., 1981. Off-fault aftershock clusters caused by shear stress increase? Bulletin of
892 the Seismological Society of America 71, 1669–1675.

893 Dempsey, E.D., Holdsworth, R.E., Imber, J., Bistacchi, A., Di Toro, G., 2014. A geological explanation
894 for intraplate earthquake clustering complexity: The zeolite-bearing fault/fracture networks in
895 the Adamello Massif (Southern Italian Alps). Journal of Structural Geology 66, 58–74.
896 https://doi.org/http://dx.doi.org/10.1016/j.jsg.2014.04.009

897 Di Toro, G., Nielsen, S., Pennacchioni, G., 2005. Earthquake rupture dynamics frozen in exhumed
898 ancient faults. Nature 436, 1009–1012.
899 https://doi.org/http://www.nature.com/nature/journal/v436/n7053/suppinfo/nature03910_S
900 1.html

901 Donath, F.A., 1961. Experimental study of shear failure in anisotropic rocks. Geological Society of
902 America Bulletin 72, 985–989. https://doi.org/10.1130/0016-
903 7606(1961)72[985:ESOSFI]2.0.CO;2

904 Dressler, B.O. & Reimold, W.U. 2004. Order or chaos? Origin and mode of emplacement of breccias
905 in floors of large impact structures. Earth-Science Reviews, 67, 1–54,
906 https://doi.org/https://doi.org/10.1016/j.earscirev.2004.01.007.

907 Edwards, M.A. & Ratschbacher, L. 2005. Seismic and aseismic weakening effects in
908 transtension: field and microstructural observations on the mechanics and architecture
909 of a large fault zone in SE Tibet. Geological Society, London, Special Publications, 245,
910 109 LP – 141, https://doi.org/10.1144/GSL.SP.2005.245.01.06.

911 Etchecopar, A., Vasseur, G. & Daignieres, M. 1981. An inverse problem in microtectonics for the
912 determination of stress tensors from fault striation analysis. Journal of Structural Geology, 3,
913 51–65, https://doi.org/https://doi.org/10.1016/0191-8141(81)90056-0.

914 Fagereng, Å. & Sibson, R.H. 2010. Mélange rheology and seismic style. Geology, 38, 751–754,
915 https://doi.org/10.1130/G30868.1.

916 Faulkner, D.R., Lewis, A.C. & Rutter, E.H. 2003. On the internal structure and mechanics of large
917 strike-slip fault zones: field observations of the Carboneras fault in southeastern Spain.
918 Tectonophysics, 367, 235–251, https://doi.org/https://doi.org/10.1016/S0040-1951(03)00134-
919 3.

920 Faulkner, D.R., Mitchell, T.M., Rutter, E.H. & Cembrano, J. 2008. On the structure and
921 mechanical properties of large strike-slip faults. Geological Society, London, Special
922 Publications, 299, 139 LP – 150, https://doi.org/10.1144/SP299.9.

923 Ferré, E.C., Yeh, E.-C., Chou, Y.-M., Kuo, R.L., Chu, H.-T. & Korren, C.S. 2016. Brushlines in fault
924 pseudotachylytes: A new criterion for coseismic slip direction. Geology , 44, 395–398,
925 https://doi.org/10.1130/G37751.1.

926 Ferré, E.C., Chou, Y.-M., Kuo, R.L., Yeh, E.-C., Leibovitz, N.R., Meado, A.L., Campbell, L., Geissman,
927 J.W., 2016. Deciphering viscous flow of frictional melts with the mini-AMS method. Journal of
928 Structural Geology 90, 15–26. https://doi.org/http://dx.doi.org/10.1016/j.jsg.2016.07.002

929 Fettes, D.J., Mendum, J.R., 1987. The evolution of the Lewisian complex in the Outer Hebrides.
930 Geological Society, London, Special Publications 27, 27–44.
931 https://doi.org/10.1144/gsl.sp.1987.027.01.04

932 Fettes, D.J., Mendum, J.R., Smith, D.I., Watson, J., 1981. 1:100 000 geological sheets (Solid): Lewis
933 and Harris, Uist and Barra. London.

934 Fettes, D.J., Mendum, J.R., Smith, D.I., Watson, J. V, 1992. Geology of the Outer Hebrides: memoir
935 for 1:100 000 geological sheets, Lewis and Harris, Uist and Barra. HMSO, London.

936 Francis, P.W., Sibson, R.H., 1973. The Outer Hebrides Thrust. In: Park, R.G., Tarney, J. (Eds.), The
937 Early Precambrian of Scotland and Related Rocks of Greenland. University of Keele, Keele, 95–
938 104.

939 Garde, A.A. and Klausen, M.B., 2016. A centnnial reappraisal of the Vredefort pseudotachylytes:
940 shaken, not stirred by mereorite impact. Journal of the Geological Society, 173, 954-965.

941 Griffith, W.A., Rosakis, A., Pollard, D.D., Ko, C.W., 2009. Dynamic rupture experiments elucidate
942 tensile crack development during propagating earthquake ruptures. Geology 37, 795–798.
943 https://doi.org/10.1130/G30064A.1

944 Gupta, S., Cowie, P.A., Dawers, N.H., Underhill, J.R., 1998. A mechanism to explain rift-basin
945 subsidence and stratigraphic patterns through fault-array evolution. Geology 26, 595–598.
946 https://doi.org/10.1130/0091-7613(1998)026<0595:AMTERB>2.3.CO;2

947 Hardman, K. 2019. Cracking Canisp: Deep void evolution during ancient
948 earthquakes. *Geoscientist,* 29*,* 10–15*,* https://doi.org/10.1144/geosci2019-003

949 Hirose, T., & Shimamoto, T. (2005). Slip-Weakening Distance of Faults during Frictional Melting as
950 Inferred from Experimental and Natural Pseudotachylytes. Bulletin of the Seismological Society
951 of America, 95(5), 1666–1673. https://doi.org/10.1785/0120040131

952

953 Hitchen, K., Stoker, M.S., Evans, D. & Beddoe-Stephens, B. 1995. Permo-Triassic sedimentary and
954 volcanic rocks in basins to the north and west of Scotland. Geological Society, London, Special
955 Publications , 91, 87–102, https://doi.org/10.1144/GSL.SP.1995.091.01.05.

956 Hoek, J.D., 1991. A classification of dyke-fracture geometry with examples from Precambrian dyke
957 swarms in the Vestfold Hills, Antarctica. Geologische Rundschau 80, 233–248.
958 https://doi.org/10.1007/bf01829363

959 Holdsworth, R.E., Selby, D., Dempsey, E., Scott, L., Hardman, K., Fallick, A.E. & Bullock, R. 2020. The
960 nature and age of Mesoproterozoic strike-slip faulting based on Re–Os geochronology of
961 syntectonic copper mineralization, Assynt Terrane, NW Scotland. Journal of the Geological
962 Society, jgs2020-011, https://doi.org/10.1144/jgs2020-011.

963 Holdsworth, R.E., van Diggelen, E.W.E., Spiers, C.J., de Bresser, J.H.P., Walker, R.J., Bowen, L., 2011.
964 Fault rocks from the SAFOD core samples: Implications for weakening at shallow depths along
965 the San Andreas Fault, California. Journal of Structural Geology 33, 132–144.
966 https://doi.org/https://doi.org/10.1016/j.jsg.2010.11.010

967 Hollingsworth, J., Ye, L. & Avouac, J.-P. 2017. Dynamically triggered slip on a splay fault in
968 the Mw 7.8, 2016 Kaikoura (New Zealand) earthquake. Geophysical Research Letters,
969 44, 3517–3525, https://doi.org/10.1002/2016GL072228.

970 Imber, J., Holdsworth, R.E., Butler, C.A., Lloyd, G.E., 1997. Fault-zone weakening processes along the
971 reactivated Outer Hebrides Fault Zone, Scotland. Journal of the Geological Society 154, 105–
972 109. https://doi.org/10.1144/gsjgs.154.1.0105

973 Imber, J., Holdsworth, R.E., Butler, C.A., Strachan, R.A., 2001. A reappraisal of the Sibson-Scholz fault
974 zone model: The nature of the frictional to viscous ("brittle-ductile") transition along a long-
975 lived, crustal-scale fault, Outer Hebrides, Scotland. Tectonics 20, 601–624.
976 https://doi.org/10.1029/2000tc001250

977 Imber, J., Strachan, R.A., Holdsworth, R.E., Butler, C.A., 2002. The initiation and early tectonic
978 significance of the Outer Hebrides Fault Zone, Scotland. Geological Magazine 139, 609–619.
979 https://doi.org/10.1017/s0016756802006969

980 Kelley, S.P., Reddy, S.M., Maddock, R., 1994. Laser-probe 40Ar/39Ar investigation of a
981 pseudotachylyte and its host rock from the Outer Isles thrust, Scotland. Geology 22, 443–446.

https://doi.org/10.1130/0091-7613(1994)022<0443:lpaaio>2.3.co;2

Kirkpatrick, J.D. & Shipton, Z.K. 2009. Geologic evidence for multiple slip weakening mechanisms during seismic slip in crystalline rock. J. Geophys. Res., 114, B12401, https://doi.org/10.1029/2008jb006037.

Krabbendam, M., Ramsay, J.G., Leslie, A.G., Tanner, P.W.G., Dietrich, D. & Goodenough, K.M. 2017. Caledonian and Knoydartian overprinting of a Grenvillian inlier and the enclosing Morar Group rocks: structural evolution of the Precambrian Proto-Moine Nappe, Glenelg, NW Scotland. Scottish Journal of Geology, 54, 13–35, https://doi.org/10.1144/sjg2017-006.

Lacombe, O., 2012. Do fault slip data inversions actually yield "paleostresses" that can be compared with contemporary stresses? A critical discussion. Comptes Rendus Geoscience 344, 159–173. https://doi.org/https://doi.org/10.1016/j.crte.2012.01.006

Lawther, S.E.M., Dempster, T.J., Shipton, Z.K. & Boyce, A.J. 2016. Effective crustal permeability controls fault evolution: An integrated structural, mineralogical and isotopic study in granitic gneiss, Monte Rosa, northern Italy. Tectonophysics, 690, 160–173, https://doi.org/https://doi.org/10.1016/j.tecto.2016.07.010.

Legros, F., Cantagrel, J. & Devouard, B. 2000. Pseudotachylyte (Frictionite) at the Base of the Arequipa Volcanic Landslide Deposit (Peru): Implications for Emplacement Mechanisms. The Journal of Geology, 108, 601–611, https://doi.org/10.1086/314421.

Lieger, D., Riller, U., & Gibson, R. L. (2009). Generation of fragment-rich pseudotachylite bodies during central uplift formation in the Vredefort impact structure, South Africa. Earth and Planetary Science Letters, 279(1–2), 53–64. https://doi.org/http://dx.doi.org/10.1016/j.epsl.2008.12.031

Lin, J., Stein, R.S., Meghraoui, M., Toda, S., Ayadi, A., Dorbath, C. & Belabbes, S. 2011. Stress transfer among en-echelon and opposing thrusts and tear faults: Triggering caused by the 2003 M w = 6.9 Zemmouri, Algeria, earthquake. Journal of Geophysical Research, 116, B03305, https://doi.org/10.1029/2010JB007654.

Lisle, R.J., 2013. Shear zone deformation determined from sigmoidal tension gashes. Journal of Structural Geology 50, 35–43. https://doi.org/https://doi.org/10.1016/j.jsg.2012.08.002

Macaudière, J., Brown, W.L., 1982. Transcrystalline shear fracturing and pseudotachylite generation in a meta-anorthosite (Harris, Scotland). Journal of Structural Geology 4, 395–406. https://doi.org/10.1016/0191-8141(82)90031-1

MacInnes, E.A., Alsop, G.I., Oliver, G.J.H., 2000. Contrasting modes of reactivation in the Outer Hebrides Fault Zone, northern Barra, Scotland. Journal of the Geological Society 157, 1009–1017. https://doi.org/10.1144/jgs.157.5.1009

Maddock, R.H., 1983. Melt origin of fault-generated pseudotachylytes demonstrated by textures. Geology 11, 105–108. https://doi.org/10.1130/0091-7613(1983)11<105:moofpd>2.0.co;2

Marrett, R., Allmendinger, R.W., 1990. Kinematic analysis of fault-slip data. Journal of Structural

Geology 12, 973–986. https://doi.org/10.1016/0191-8141(90)90093-E

McCoss, A. M. (1986). Simple constructions for deformation in transpression/transtension zones. Journal of Structural Geology, 8(6), 715–718. https://doi.org/https://doi.org/10.1016/0191-8141(86)90077-5

Mitchell, T.M., Toy, V., Di Toro, G., Renner, J., Sibson, R.H., 2016. Fault welding by pseudotachylyte formation. Geology . https://doi.org/10.1130/G38373.1

Mohr-Westheide, T. & Reimold, W.U. 2011. Formation of pseudotachylitic breccias in the central uplifts of very large impact structures: Scaling the melt formation. Meteoritics & Planetary Science, 46, 543–555, https://doi.org/10.1111/j.1945-5100.2011.01173.x.

Moir, H., Lunn, R.J., Shipton, Z.K. & Kirkpatrick, J.D. 2010. Simulating brittle fault evolution from networks of pre-existing joints within crystalline rock. Journal of Structural Geology, 32, 1742–1753, https://doi.org/https://doi.org/10.1016/j.jsg.2009.08.016.

Nemcok, M., Lisle, R.J., 1995. A stress inversion procedure for polyphase fault/slip data sets. Journal of Structural Geology 17, 1445–1453. https://doi.org/https://doi.org/10.1016/0191-8141(95)00040-K

Ngo, D., Huang, Y., Rosakis, A., Griffith, W.A., Pollard, D., 2012. Off-fault tensile cracks: A link between geological fault observations, lab experiments, and dynamic rupture models. Journal of Geophysical Research: Solid Earth 117, B01307. https://doi.org/10.1029/2011jb008577

Nicholson, R., Pollard, D.D., 1985. Dilation and linkage of echelon cracks. Journal of Structural Geology 7, 583–590. https://doi.org/https://doi.org/10.1016/0191-8141(85)90030-6

Nicol, A., Walsh, J.J., Watterson, J., Underhill, J.R., 1997. Displacement rates of normal faults. Nature 390, 157–159.

Nielsen, S., Mosca, P., Giberti, G., Di Toro, G., Hirose, T., & Shimamoto, T. (2010). On the transient behavior of frictional melt during seismic slip. Journal of Geophysical Research, 115(B10), B10301. https://doi.org/10.1029/2009JB007020

Nüchter, J.-A. & Ellis, S. 2011. Mid-crustal controls on episodic stress-field rotation around major reverse, normal and strike-slip faults. Geological Society, London, Special Publications, 359, 187–201, https://doi.org/10.1144/sp359.11.

O'Callaghan, J.W. & Osinski, G.R. 2019. Geochemical and petrographic variations in pseudotachylyte along the Outer Hebrides Fault Zone, Scotland. Journal of the Geological Society, 177, 50–65, https://doi.org/10.1144/jgs2019-009.

Olson, J.E., Pollard, D.D., 1991. The initiation and growth of en échelon veins. Journal of Structural Geology 13, 595–608. https://doi.org/https://doi.org/10.1016/0191-8141(91)90046-L

Orife, T., Lisle, R.J., 2006. Assessing the statistical significance of palaeostress estimates: simulations using random fault-slips. Journal of Structural Geology 28, 952–956.

https://doi.org/https://doi.org/10.1016/j.jsg.2006.03.005

Osinski, G.R., I, A.G., Oliver, G.J.H., 2001. Extensional tectonics of the Outer Hebrides Fault Zone, South Uist, northwest Scotland. Geological Magazine 138, 325–344.

Philpotts, A.R., 1964. Origin of pseudotachylites. American Journal of Science 262, 1008–1035. https://doi.org/10.2475/ajs.262.8.1008

Piper, J.D.A. 1992. Post-Laxfordian magnetic imprint in the Lewisian metamorphic complex and strike-slip motion in the Minches, NW Scotland. Journal of the Geological Society, 149, 127–137, https://doi.org/10.1144/gsjgs.149.1.0127.

Pollard, D.D., Segall, P., Delaney, P.T., 1982. Formation and interpretation of dilatant echelon cracks. Geological Society of America Bulletin 93, 1291–1303. https://doi.org/10.1130/0016-7606(1982)93<1291:FAIODE>2.0.CO;2

Reddy, S.M., Johnson, T.E., Fischer, S., Rickard, W.D.A. & Taylor, R.J.M. 2015. Precambrian reidite discovered in shocked zircon from the Stac Fada impactite, Scotland. Geology, 43, 899–902.

Rickard, M.J., Rixon, L.K., 1983. Stress configurations in conjugate quartz-vein arrays. Journal of Structural Geology 5, 573–578. https://doi.org/http://dx.doi.org/10.1016/0191-8141(83)90069-X

Roberts, A.M., Holdsworth, R.E., 1999. Linking onshore and offshore structures: Mesozoic extension in the Scottish Highlands. Journal of the Geological Society 156, 1061–1064.

Ross, Z.E., Hauksson, E., Ben-Zion, Y., 2017. Abundant off-fault seismicity and orthogonal structures in the San Jacinto fault zone. Science Advances 3.

Rowe, C.D., Griffith, W.A., 2015. Do faults preserve a record of seismic slip: A second opinion. Journal of Structural Geology 78, 1–26. https://doi.org/http://dx.doi.org/10.1016/j.jsg.2015.06.006

Rowe, C.D., Ross, C., et al. 2018. Geometric Complexity of Earthquake Rupture Surfaces Preserved in Pseudotachylyte Networks. Journal of Geophysical Research: Solid Earth, 123, 7998–8015, https://doi.org/10.1029/2018JB016192.

Sato, K., Yamaji, A., 2006. Embedding stress difference in parameter space for stress tensor inversion. Journal of Structural Geology 28, 957–971. https://doi.org/https://doi.org/10.1016/j.jsg.2006.03.004

Schulz, S.E. & Evans, J.P. 2000. Mesoscopic structure of the Punchbowl Fault, Southern California and the geologic and geophysical structure of active strike-slip faults. Journal of Structural Geology, 22, 913–930, https://doi.org/https://doi.org/10.1016/S0191-8141(00)00019-5.

Shan, Y., Fry, N., 2005. A hierarchical cluster approach for forward separation of heterogeneous fault/slip data into subsets. Journal of Structural Geology 27, 929–936. https://doi.org/https://doi.org/10.1016/j.jsg.2005.02.001

Sherlock, S.C., Jones, K.A. & Park, R.G. 2008. Grenville-age pseudotachylite in the Lewisian: laserprobe 40Ar/39Ar ages from the Gairloch region of Scotland (UK). Journal of the Geological Society, 165, 73–83, https://doi.org/10.1144/0016-76492006-134.

Sherlock, S.C., Strachan, R.A., Jones, K.A., 2009. High spatial resolution 40Ar/39Ar dating of pseudotachylites: geochronological evidence for multiple phases of faulting within basement gneisses of the Outer Hebrides (UK). Journal of the Geological Society 166, 1049–1059. https://doi.org/10.1144/0016-76492008-125

Sibson, R.H., 1980. Transient discontinuities in ductile shear zones. Journal of Structural Geology 2, 165–171. https://doi.org/10.1016/0191-8141(80)90047-4

Sibson, R.H., 1977a. Fault rocks and fault mechanisms. Journal of the Geological Society 133, 191–213. https://doi.org/10.1144/gsjgs.133.3.0191

Sibson, R.H., 1977b. The Outer Hebrides Thrust: Its structure, mechanism and deformation environment. University of London.

Sibson, R.H., 1975. Generation of peseudotachylyte by ancient seismic faulting. Geophysical Journal of the Royal Astronomical Society 43, 775. https://doi.org/10.1111/j.1365-246X.1975.tb06195.x

Simms, M.J. 2020. Discussion on 'The Mesoproterozoic Stac Fada proximal ejecta blanket, NW Scotland: constraints on crater location from field observations, anisotropy of magnetic susceptibility, petrography and geochemistry', Journal of the Geological Society, London, 176, 830–846. Journal of the Geological Society, 177, 449 LP – 451, https://doi.org/10.1144/jgs2019-155.

Simms, M.J. & Ernstson, K. 2019. A reassessment of the proposed 'Lairg Impact Structure' and its potential implications for the deep structure of northern Scotland. Journal of the Geological Society, 176, 817 LP – 829, https://doi.org/10.1144/jgs2017-161.

Simón, J.L., 2018. Forty years of paleostress analysis: has it attained maturity? Journal of Structural Geology. https://doi.org/https://doi.org/10.1016/j.jsg.2018.02.011

Smythe, D.K., Dobinson, A., McQuillin, R., Brewer, J.A., Matthews, D.H., Blundell, D.J., Kelk, B., 1982. Deep structure of the Scottish Caledonides revealed by the MOIST reflection profile. Nature 299, 338–340.

Spray, J.G., 1998. Localized shock- and friction-induced melting in response to hypervelocity impact. In Meteorites: Flux with Time and Impact Effects, ed. MM Grady, R Hutchinson, GJH McCall, DA Rothery, pp. 171–80. Geol. Soc. London Spec. Pub. 140:171–80

Spray, J.G., 2010. Frictional Melting Processes in Planetary Materials: From Hypervelocity Impact to Earthquakes. In: Jeanloz, R., Freeman, K.H. (Eds.), Annual Review of Earth and Planetary Sciences 38, 221–254. https://doi.org/10.1146/annurev.earth.031208.100045

Streule, M.J., Strachan, R.A., Searle, M.P., Law, R.D., 2010. Comparing Tibet-Himalayan and Caledonian crustal architecture, evolution and mountain building processes. Geological Society, London, Special Publications 335, 207–232. https://doi.org/10.1144/sp335.10

1129 Szulc, A.G., Alsop, G.I., Oliver, G.J.H., 2008. Kinematic and thermal constraints on the reactivation of
1130 the Outer Hebrides Fault Zone, NW Scotland. Geological Magazine 145, 623–636.
1131 https://doi.org/10.1017/S0016756808004925

1132 Thompson, L.M. & Spray, J.G. 1992. Pseudotachylytic rock distribution and genesis within the
1133 Sudbury impact structure. Geological Society of America Special Papers , 293, 275–288,
1134 https://doi.org/10.1130/SPE293-p275.

1135 Tien, Y.M., Kuo, M.C. & Juang, C.H. 2006. An experimental investigation of the failure mechanism of
1136 simulated transversely isotropic rocks. International Journal of Rock Mechanics and Mining
1137 Sciences, 43, 1163–1181, https://doi.org/https://doi.org/10.1016/j.ijrmms.2006.03.011.

1138 Wallace, R.E., 1951. Geometry of Shearing Stress and Relation to Faulting. The Journal of Geology 59,
1139 118–130. https://doi.org/10.1086/625831

1140 Wallis, D., Lloyd, G.E., Phillips, R.J., Parsons, A.J., Walshaw, R.D., 2015. Low effective fault strength
1141 due to frictional-viscous flow in phyllonites, Karakoram Fault Zone, NW India. Journal of
1142 Structural Geology 77, 45–61. https://doi.org/http://dx.doi.org/10.1016/j.jsg.2015.05.010

1143 Wallis, D., Phillips, R.J., Lloyd, G.E., 2013. Fault weakening across the frictional-viscous transition
1144 zone, Karakoram Fault Zone, NW Himalaya. Tectonics 32, 1227–1246.
1145 https://doi.org/10.1002/tect.20076

1146 Walsh, J.J., Childs, C., Imber, J., Manzocchi, T., Watterson, J., Nell, P.A.R., 2003. Strain localisation
1147 and population changes during fault system growth within the Inner Moray Firth, Northern
1148 North Sea. Journal of Structural Geology 25, 307–315.
1149 https://doi.org/http://dx.doi.org/10.1016/S0191-8141(02)00028-7

1150 White, J.C., 1996. Transient discontinuities revisited: pseudotachylyte, plastic instability and the
1151 influence of low pore fluid pressure on deformation processes in the mid-crust. Journal of
1152 Structural Geology 18, 1471–1486. https://doi.org/10.1016/s0191-8141(96)00059-4

1153 White, S.H., Glasser, J., 1987. The Outer Hebrides Fault Zone: evidence for normal movements.
1154 Geological Society, London, Special Publications 27, 175–183.
1155 https://doi.org/10.1144/gsl.sp.1987.027.01.15

1156 Whitehouse, M.J. & Bridgwater, D. 2001. Geochronological constraints on Paleoproterozoic crustal
1157 evolution and regional correlations of the northern Outer Hebridean Lewisian complex,
1158 Scotland. Precambrian Research, 105, 227–245,
1159 https://doi.org/http://dx.doi.org/10.1016/S0301-9268(00)00113-3.

1160 Xu, S.-S., Nieto-Samaniego, A.F. and Alaniz-Álvarez, S.A. 2009. Quantification of true displacement
1161 using apparent displacement along an arbitrary line on a fault plane. Tectonophysics 467, 107–118.

1162 Yamada, E. & Sakaguchi, K. 1995. Fault-slip calculation from separations. Journal of
1163 Structural Geology, 17, 1065–1070, https://doi.org/https://doi.org/10.1016/0191-
1164 8141(95)00003-V.

1165 Žalohar, J., Vrabec, M., 2007. Paleostress analysis of heterogeneous fault-slip data: The Gauss

method. Journal of Structural Geology 29, 1798–1810.
https://doi.org/https://doi.org/10.1016/j.jsg.2007.06.009

1169

Deformation phase	Kinematics	Deformation style and fault rock types	Location(s) observed	Reference
Pre-Caledonian (Late Laxfordian, 1.7 Ga, or Grenvillian, 1.1 Ga)	Top-to-NW thrusting	Ductile shear	Lewis & Harris	Butler et al. (1995) Imber et al. (2001)
	Top-to-E extension (?)	Observed only as offshore growth strata in Torridon Group	Much of OHFZ	Imber et al. (2001)
Caledonian compression	Top-to NW thrusting	Ductile shear	Lewis & Harris	Sibson (1977)
			South Uist	Osinski et al. (2001)
			Barra	MacInnes et al. (2000)
	Top-to NNW/NW/WNW (E-W compression?)	Brittle thrust faulting (cataclasites and pseudotachylytes)	Much of OHFZ	Imber et al. (2001) Butler et al. (1998) Sibson (1977)
			South Uist	Osinski et al. (2001)
			Barra	MacInnes et al. (2000)
(Late) Caledonian strike-slip	Top-to-NE sinistral (oblique)	Phyllonite shear zones	Scalpay	Szulc et al. (2008)
			Much of OHFZ	Imber et al. (2001) Butler et al. (1998)
	Dextral and sinistral (limited observations)	Small displacement slip surfaces along phyllonite foliation	South Uist	Osinski et al. (2001)
	Dextral and sinistral	Brittle faulting (with pseudotachylytes)	Barra	MacInnes et al. (2000)
Late Caledonian extension	Top-to-S, -E or SE extensional	Shear of phyllonites and brittle slip along phyllonite foliation	Much of OHFZ	Imber et al. (2001)
	Top-to-ENE, -NE and top-to-ESE extensional	Shear of phyllonites, brittle faults (with pseudotachylytes), localised detachment faults	South Uist	Osinski et al. (2001)
	Top-to-ESE and	Shear of phyllonites, steep brittle faults	Barra	MacInnes et al.

	–E extensional	(with pseudotachylytes) and shallow detachments		(2000)

Table. 1: Existing structural framework for deformation along the OHFZ

Figure 1. Geological map of the Outer Hebrides (Western Isles), UK, showing key lithological units (after Fettes et al., 1981) and location of faults relevant to discussion (selected from Sibson, 1977b; Fettes et al., 1981, 1992; Brewer and Smythe, 1986). Indication of pseudotachylyte localities shown by black circles (selected from Fettes et al., 1992; MacInnes et al., 2000, plus those observed in current study). Stereonets (lower hemisphere, equal area) show poles-to-planes of pseudotachylyte generation planes; top left plot covers the whole OHFZ region whilst additional plots are subset by local region. Kamb contours show density increments as indicated in the respective legend. The regional dip of the OHFZ is indicated on each plot via a black great-circle and black pole whilst the local trend for each region is indicated by grey ticks.

Figure 2. Typical features of OHFZ pseudotachylytes. (a) Pseudotachylyte fault vein (generation plane) and injections into host rock, North Uist [BNG 86113 86662]; (b) Fault breccia with pseudotachylyte matrix, South Uist [BNG 75692 823056]; (c) Back-scattered electron image of pseudotachylyte vein displaying radiating plagioclase microlites around unmelted clasts of quartz and plagioclase, within ultrafine matrix of plagioclase, hornblende, biotite and iron oxide; (d) back-scattered electron image of pseudotachylyte ('PST') vein margin with strong spherulitic texture.

Figure 3. Field and microstructural evidence for slip sense on pseudotachylyte faults. (a) pseudotachylyte fault displaying apparent normal, top-down-to-south east displacement of shallower-dipping pseudotachylyte vein [BNG 130028 917107]; (b) Overlay over (a) illustrating the two phases of pseudotachylyte; (c) pseudotachylyte faults with apparent reverse top-to-NE and top-to-SW offset of amphibolite layers [BNG 85626 856188]; (d) Overlay over (c) showing thin pseudotachylyte faults offsetting amphibolite banding; (e) Backscattered electron image of pseudotachylyte ('PST') vein with shape preferred orientation of quartz (darker grey) and plagioclase clasts suggesting top-to-left (east) apparent slip; (f) Cataclasic margin within vein with S-C type foliation picked out by pseudotachylyte ingress indicating top-to-left slip (top-to-SW).

Figure 4. Dynamic off-fault tensile crack model for pseudotachylyte injection veins. (a) Sequence of near-parallel injection veins (arrowed) restricted to single wall of pseudotachylyte fault [BNG 30388 16447]; (b) Overlay over (a) showing pseudotachylyte fault and injection vein geometry; (c) Sequence of inclined near-parallel injection veins restricted to single wall of pseudotachylyte fault [BNG 65624 803536]; (d) Overlay over (c) showing pseudotachylyte fault and injection vein geometry; (e) Model of dynamic tensile injections showing how local rupture tip stress fields can induce coseismic tensile cracking (after Dalguer et al., 2003); (f) Determination of slip plunge and azimuth (white arrow) from the resolved normal to the injection vein dip, and slip sense from identifying the acute angle between injection veins and the fault plane.

Figure 5. En-echelon injection vein systems. (a) cross-cutting arrays of pseudotachylyte injection veins [horizontal section, BNG 66008 803981]; (b) Diffuse array of en-echelon veins [horizontal section, BNG 65687 803437]; (c) Linear array of en-echelon veins [horizontal section, BNG 70537 799802]; (d) Example of pseudotachylyte fault vein with injection vein segmenting at injection tip [vertical section, BNG 79497 810173]; (e) Pebble rotated 180° to show segmentation of single injection vein into en-echelon system.

Figure 6. Model of en-echelon pseudotachylyte injection vein formation. (a) Planar tensile fracture (or injection vein) propagating with no deviation in stress field; (b) En-echelon segmentation of fracture (or injection vein) in response to shear experienced at the propagating tip. Such mixed mode behaviour can form a response to a spatial and/or temporal change in stress field orientation (after Clemente et al., 2007); (c) Application of the en-echelon model to a dynamic tensile pseudotachylyte injection vein propagating away from the fault plane. Initially the vein is oriented relative to the slip direction and the dynamic rupture tip stress field, but this influence falls away as the rupture tip moves on and the injection vein propagates away from the fault.

Figure 7. Apparent slip sense and fault dip observed from offset markers across pseudotachylyte fault veins in the field (n = 29) and microstructural indicators from fault veins observed in thin section, where the vein orientation was known (n = 7).

Figure 8. Large stereonets (right hand side) show the stress fields resulting from palaeostress analysis and the faults that are mechanically attributable to them. Hangingwall slip directions are indicated with arrows. The relative stress state for the faults attributable to each stress field is shown plotted on a dimensionless Mohr's circle to confirm the mechanical compatibility. The fault plane solutions for individual faults in the dataset are plotted with the fault plane in bold black. These slip solutions (focal mechanisms) are block-coloured to correspond to the stress field with which they are attributable to - grey shaded solutions were not compatible with any of the resulting stress fields (* indicates a slip solution which is mechanically attributable to both the orange and the pink stress fields). Also shown is the fault plane solution resulting from AMS analysis (Ferré et al., 2016). Turquoise shading on the map indicates presence of phyllonite belts (after Imber, 1998).

Figure 9. Results from en-echelon array observations: (a) Orientation of perpendicular to en-echelon arrays (array-normals); (b) orientation of perpendicular to en-echelon segments (segment-normals); (c) magnitude and direction of segment rotation relative to the parent array/vein, by array orientation.

Figure 10. Maps of localities where multiple en-echelon arrays are observed, indicating the segment-normal (the propagation trajectory of which is rotating to be compliant with σ_3) and the sense of deviation (clockwise or anticlockwise) relative to the whole en-echelon array. Geological units after Fettes et al. (1981); base maps from © OpenStreetMap contributors (https://www.openstreetmap.org/copyright).

Figure 11. Acute angle between pseudotachylyte-bearing fault and surrounding foliation (n = 67).

Figure 12. Schematic illustration of deformation events which may have contributed to the record of seismic ruptures around the Outer Hebrides, resulting in the record of scattered and variously oriented pseudotachylyte – bearing faults. Suggested stress fields are sourced from palaeostress analysis (Fig. 8). Dates for meteorite impact are taken from Reddy et al. (2015) and for early mainland faulting from Sherlock et al. (2009) and Holdsworth et al. (2020).

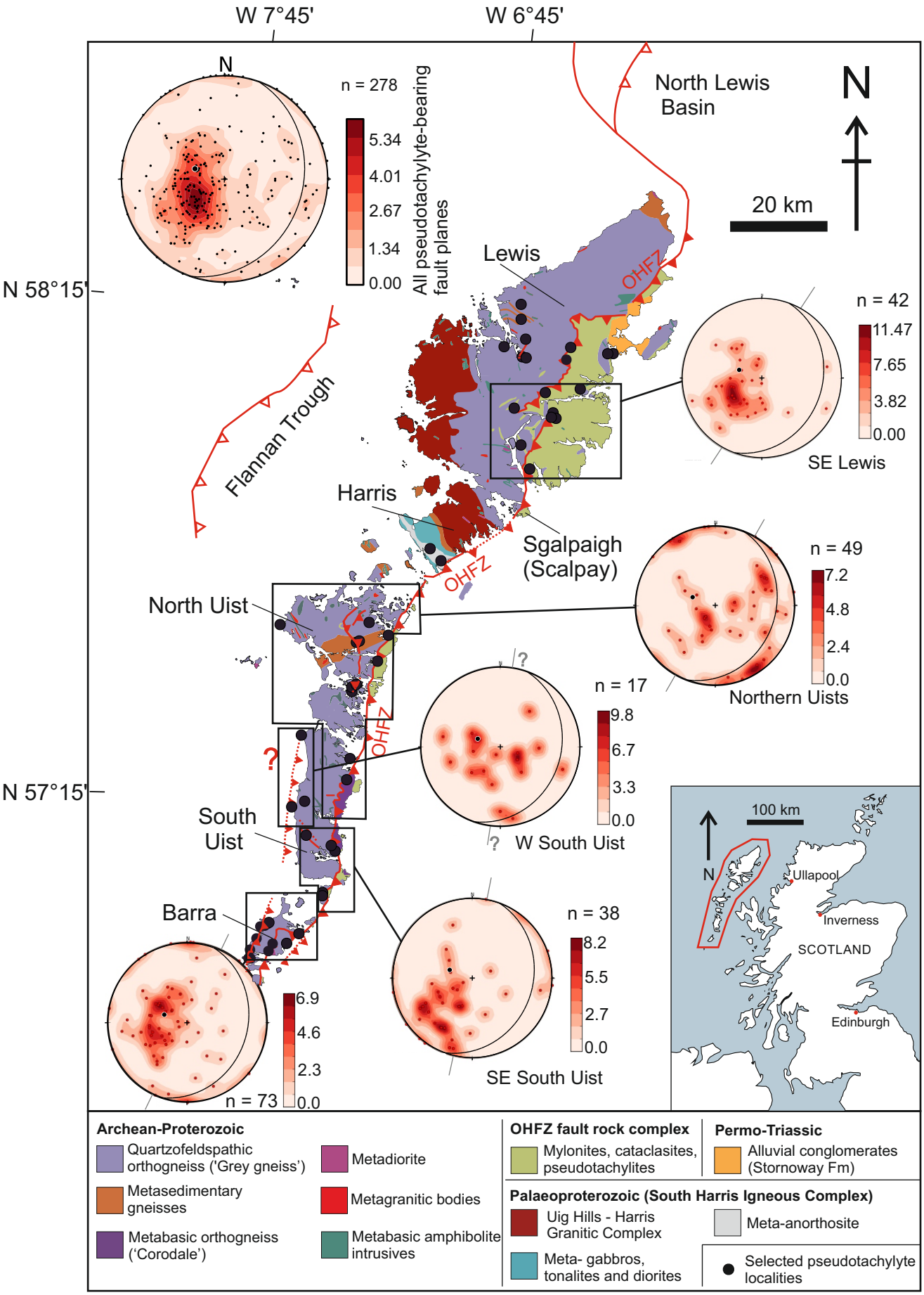
W 7°45'
W 6°45'
N 58°15'
N 57°15'
N
n = 278
5.34
4.01
2.67
1.34
0.00
All pseudotachylyte-bearing fault planes
North Lewis Basin
N
20 km
Lewis
OHFZ
Flannan Trough
n = 42
11.47
7.65
3.82
0.00
SE Lewis
Harris
Sgalpaigh (Scalpay)
OHFZ
n = 49
7.2
4.8
2.4
0.0
Northern Uists
North Uist
OHFZ
?
n = 17
9.8
6.7
3.3
0.0
W South Uist
South Uist
Barra
n = 38
8.2
5.5
2.7
0.0
SE South Uist
6.9
4.6
2.3
0.0
n = 73
100 km
N
Ullapool
Inverness
SCOTLAND
Edinburgh
Archean-Proterozoic
Quartzofeldspathic orthogneiss ('Grey gneiss')
Metasedimentary gneisses
Metabasic orthogneiss ('Corodale')
Metadiorite
Metagranitic bodies
Metabasic amphibolite intrusives
OHFZ fault rock complex
Mylonites, cataclasites, pseudotachylites
Permo-Triassic
Alluvial conglomerates (Stornoway Fm)
Palaeoproterozoic (South Harris Igneous Complex)
Uig Hills - Harris Granitic Complex
Meta-anorthosite
Meta- gabbros, tonalites and diorites
Selected pseudotachylyte localities

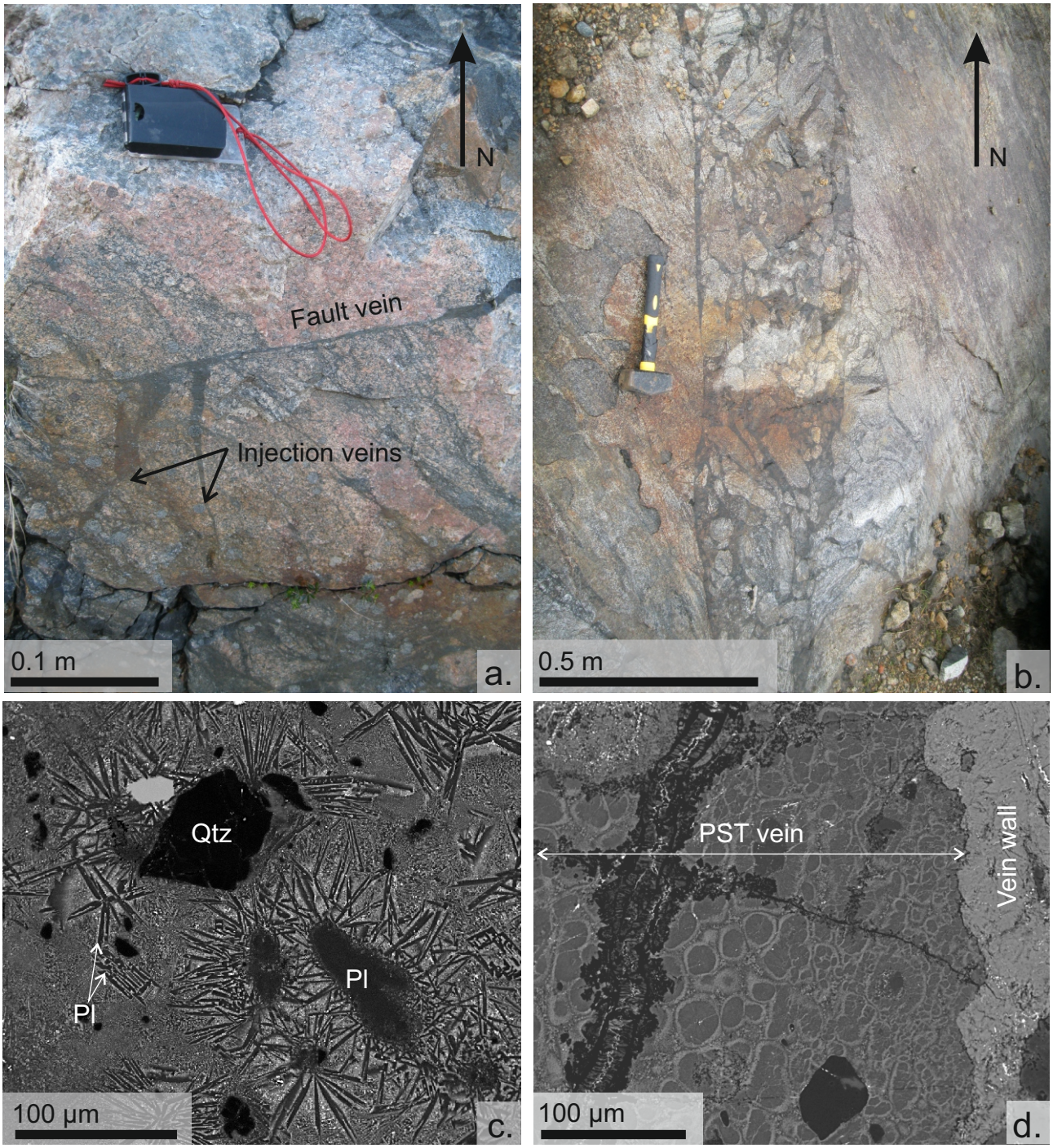
N
Fault vein
Injection veins
0.1 m
a.
N
0.5 m
b.
Qtz
Pl
Pl
100 µm
c.
PST vein
Vein wall
100 µm
d.

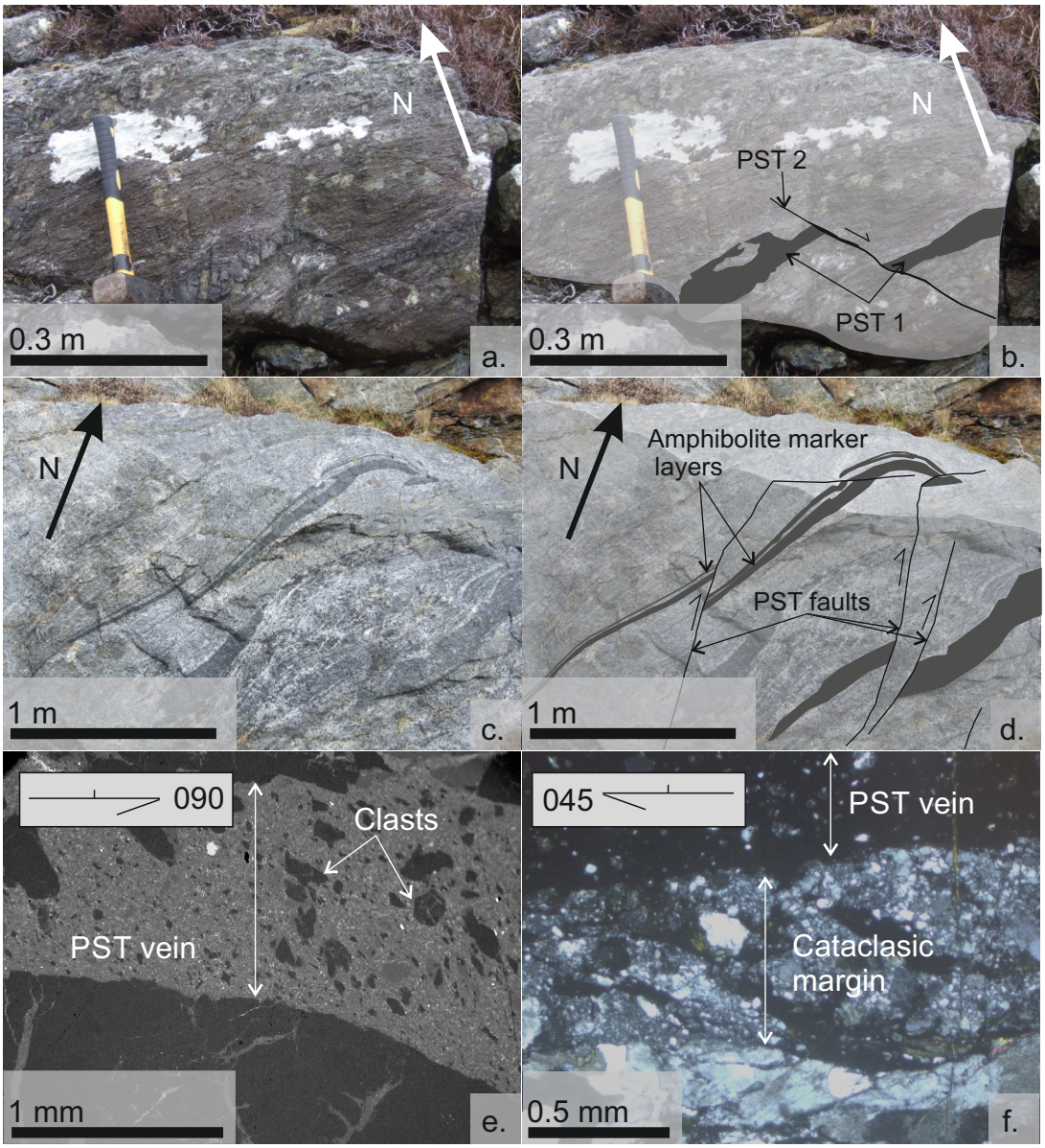
N
0.3 m
a.
N
PST 2
PST 1
0.3 m
b.
N
1 m
c.
N
Amphibolite marker layers
PST faults
1 m
d.
090
Clasts
PST vein
1 mm
e.
045
PST vein
Cataclasic margin
0.5 mm
f.

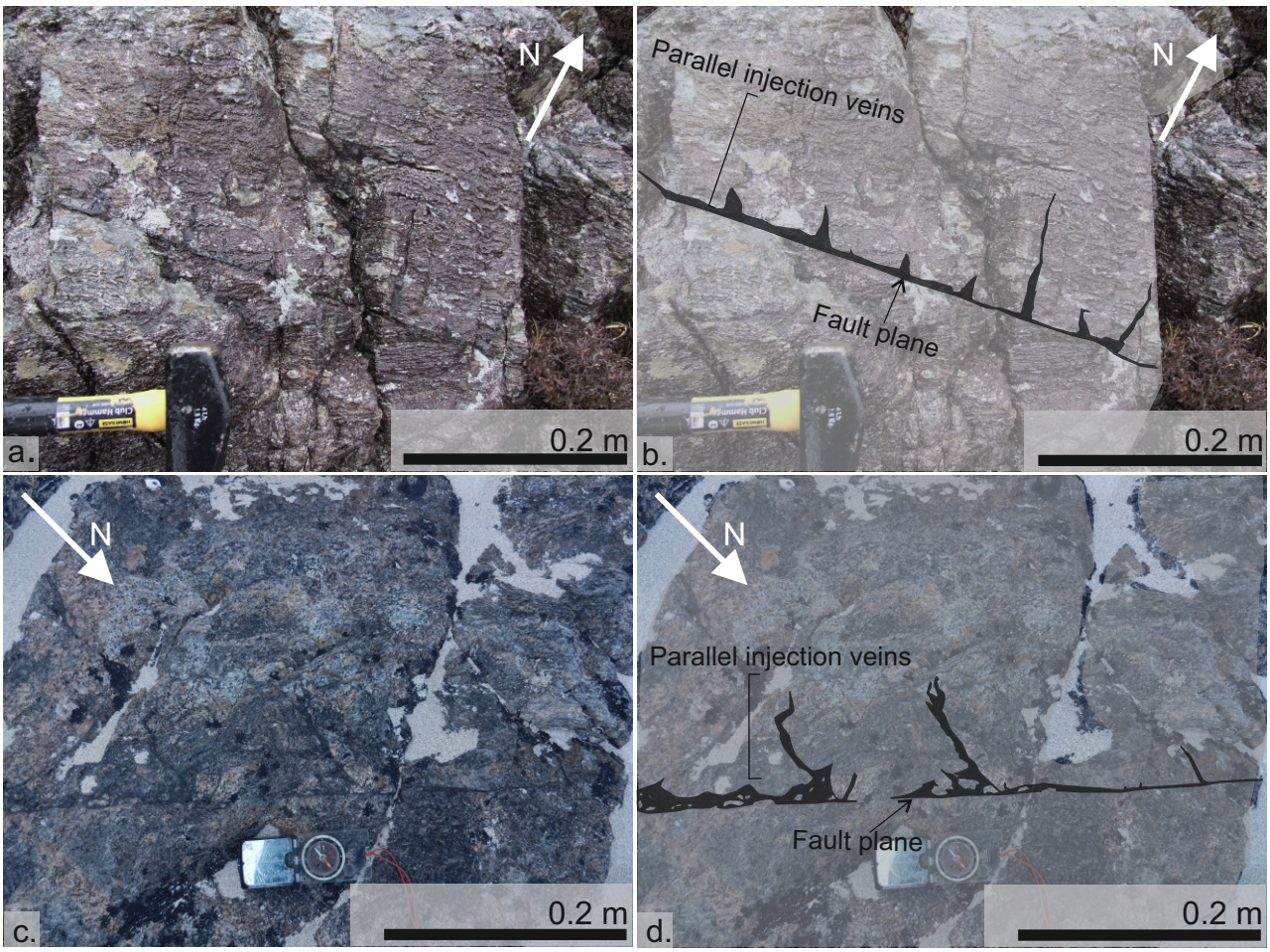
N
0.2 m
a.
Parallel injection veins
Fault plane
b.
c.
d.

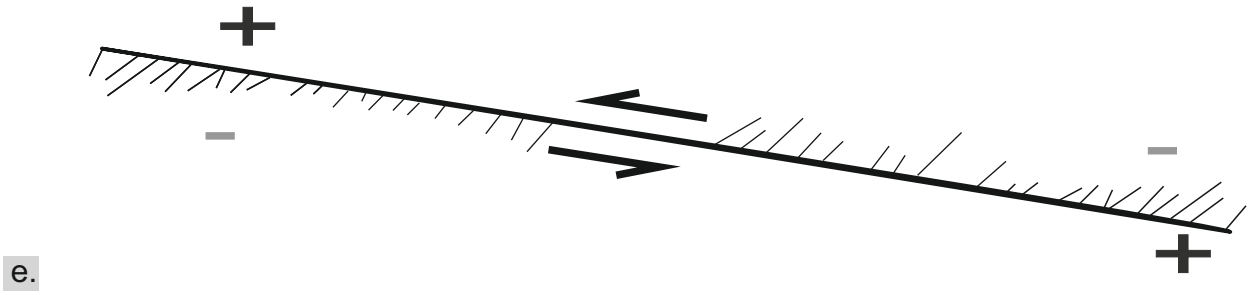
+
−
−
+

e.

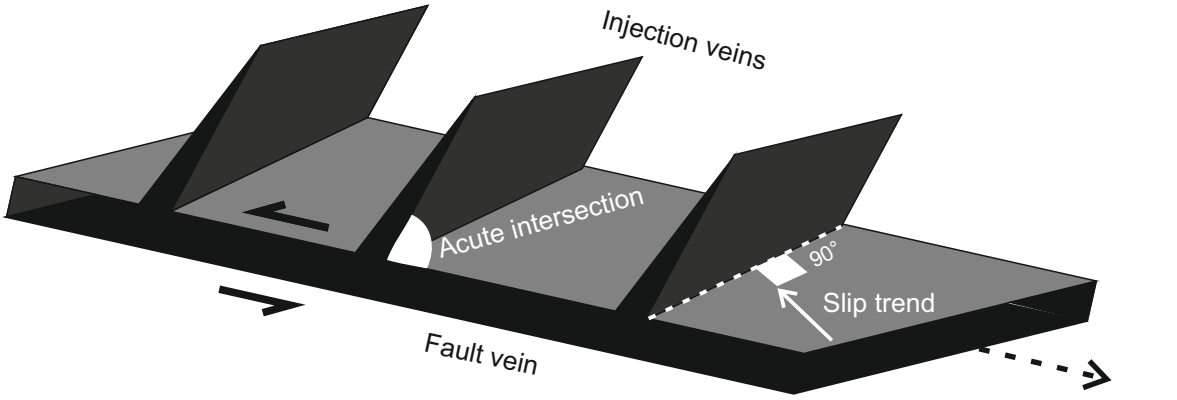
Injection veins
Acute intersection
90°
Slip trend
Fault vein
Propagation direction

f.


a.
N
0.3 m
b.
N
0.1 m
c.
N
0.1 m
d.
vertical exposure
face strikes ~070-250
segmented at
injection tip
'parent'
injection vein
PST fault vein
0.2 m
e.
5 cm

Planar fracture

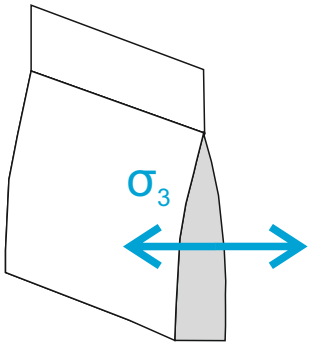

a. Mode I

En-echelon segments

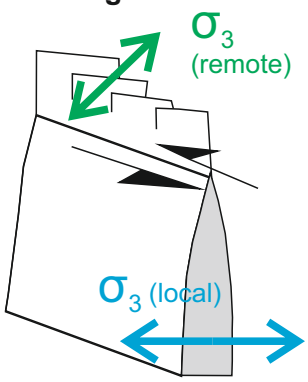

b. Mixed mode (I, III)

En echelon pseudotachylyte injection veins

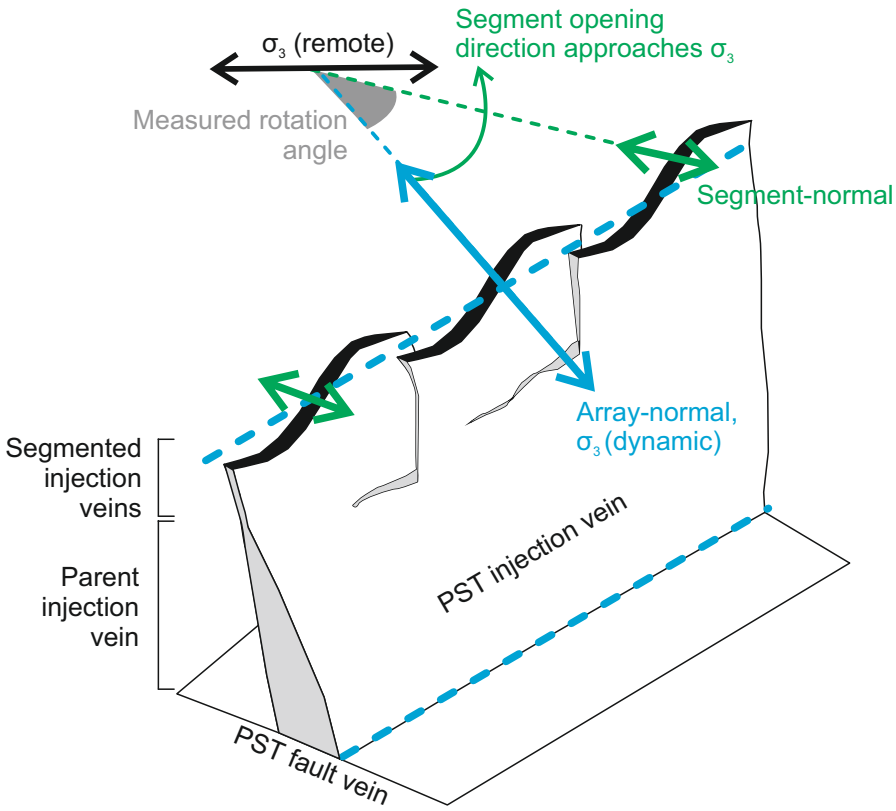

c.

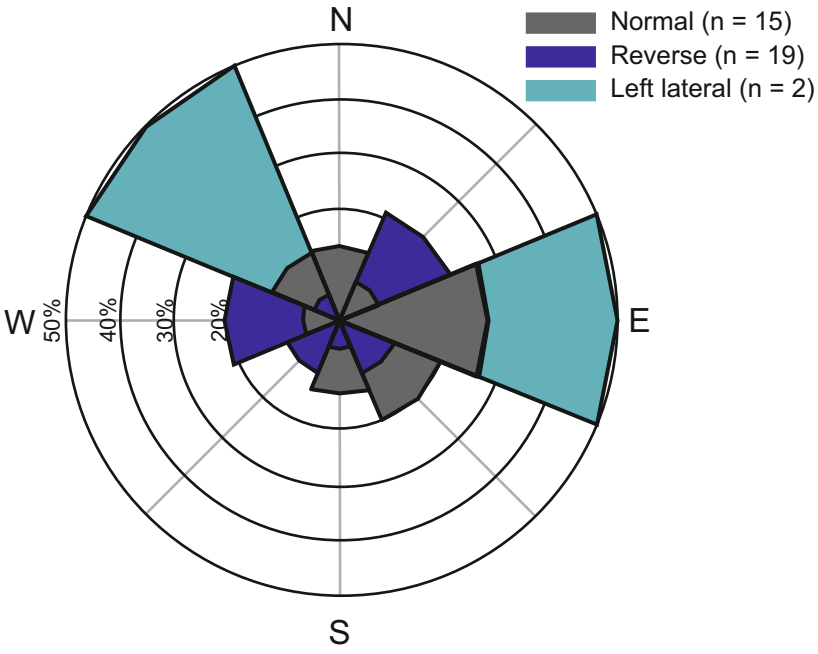
N
E
S
W
50%
40%
30%
20%
Normal (n = 15)
Reverse (n = 19)
Left lateral (n = 2)

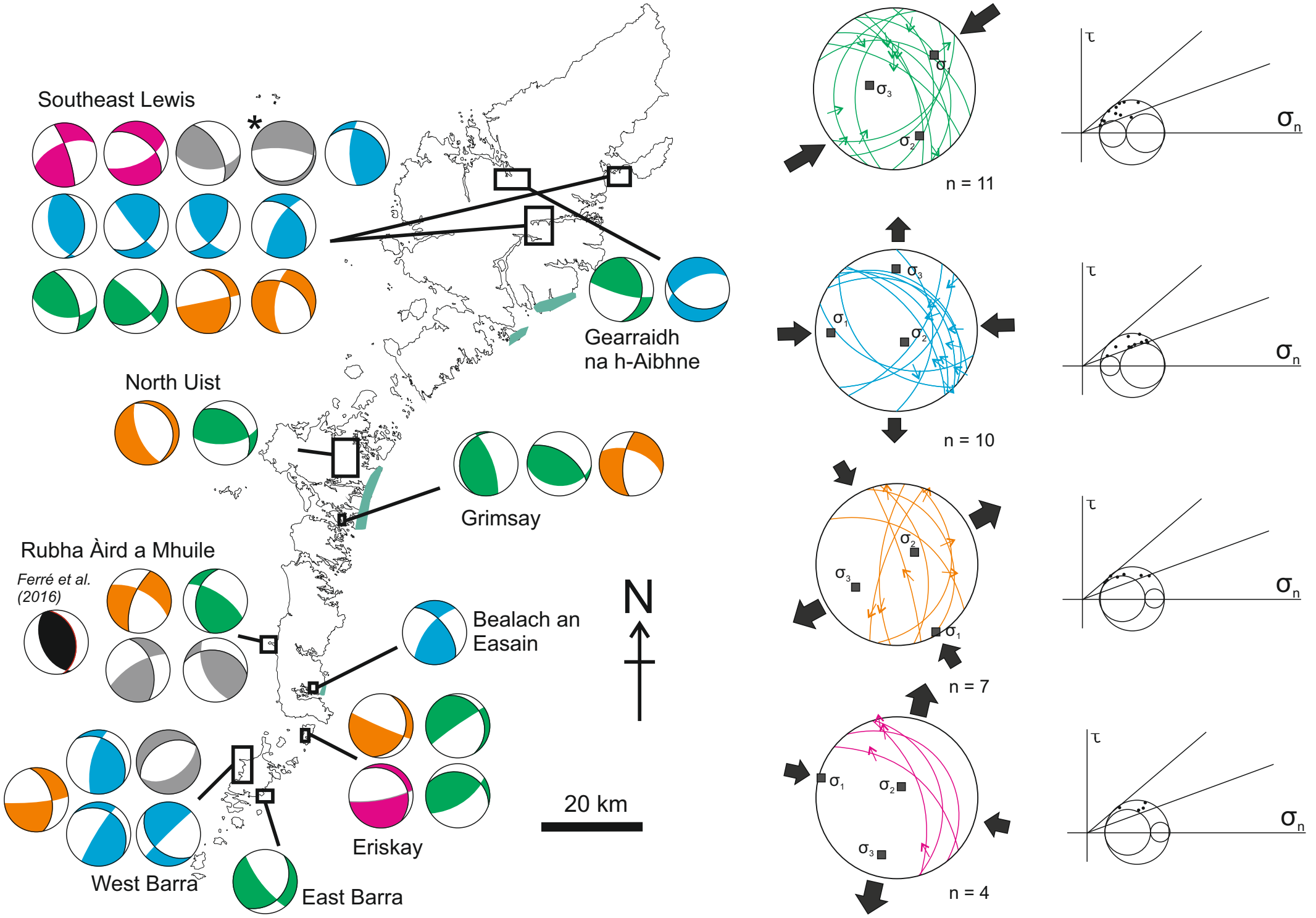
Southeast Lewis
Gearraidh
na h-Aibhne
North Uist
Grimsay
Rubha Àird a Mhuile
Ferré et al.
(2016)
Bealach an
Easain
N
20 km
Eriskay
West Barra
East Barra
σ1
σ2
σ3
n = 11
n = 10
n = 7
n = 4
τ
σn

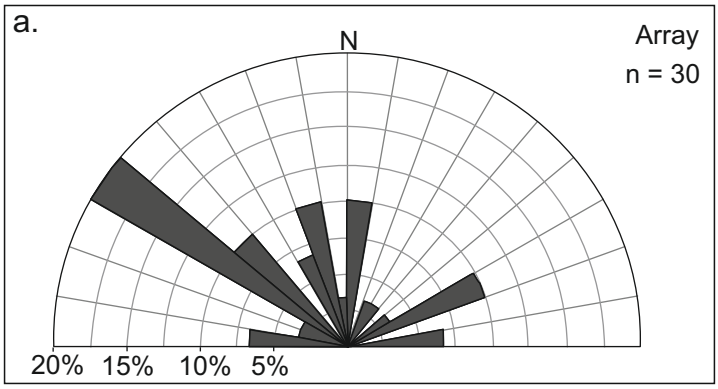
a.
N
Array
n = 30
20%
15%
10%
5%

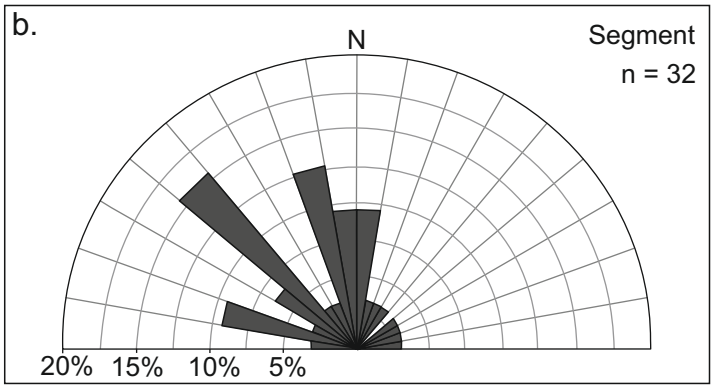
b.
N
Segment
n = 32
20%
15%
10%
5%

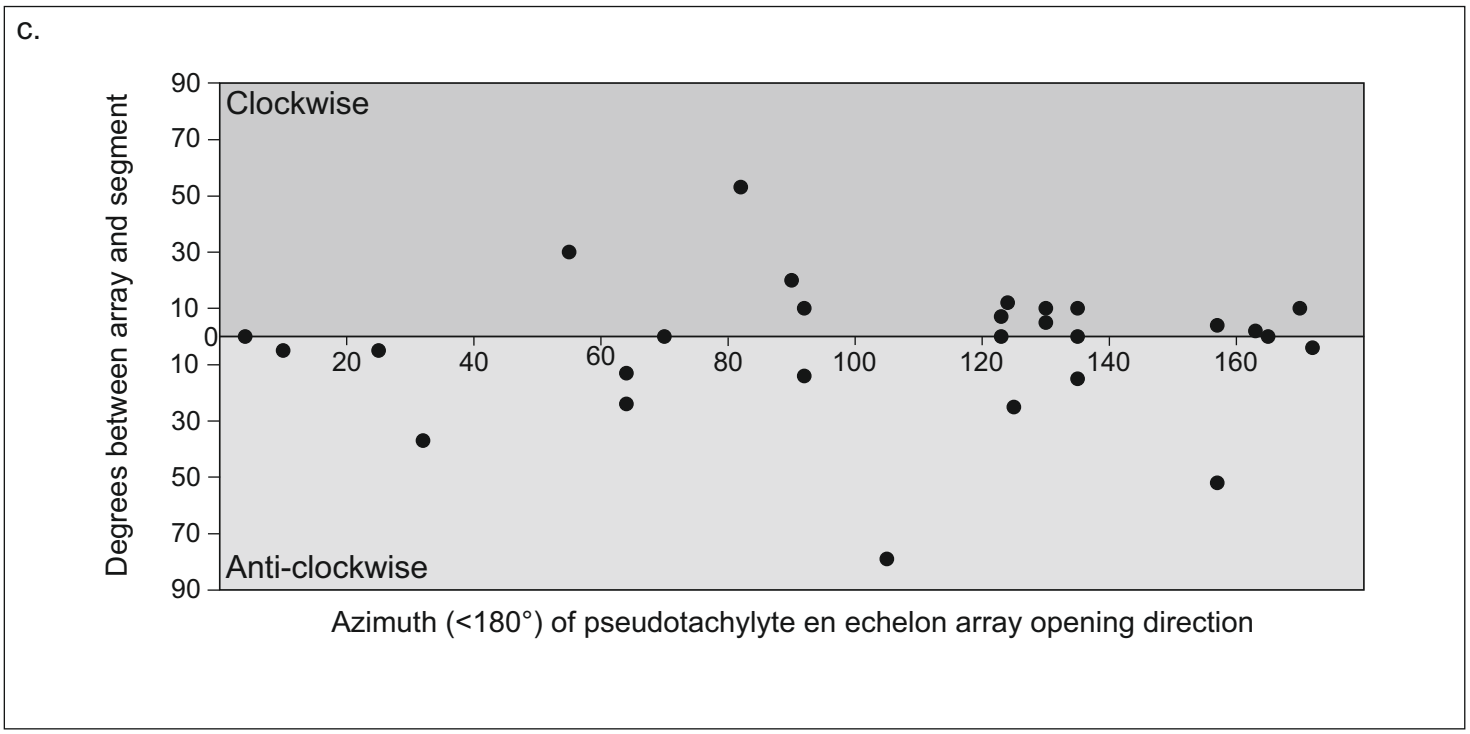
c.
Clockwise
Anti-clockwise
Degrees between array and segment
90
70
50
30
10
0
10
30
50
70
90
20
40
60
80
100
120
140
160
Azimuth (<180°) of pseudotachylyte en echelon array opening direction

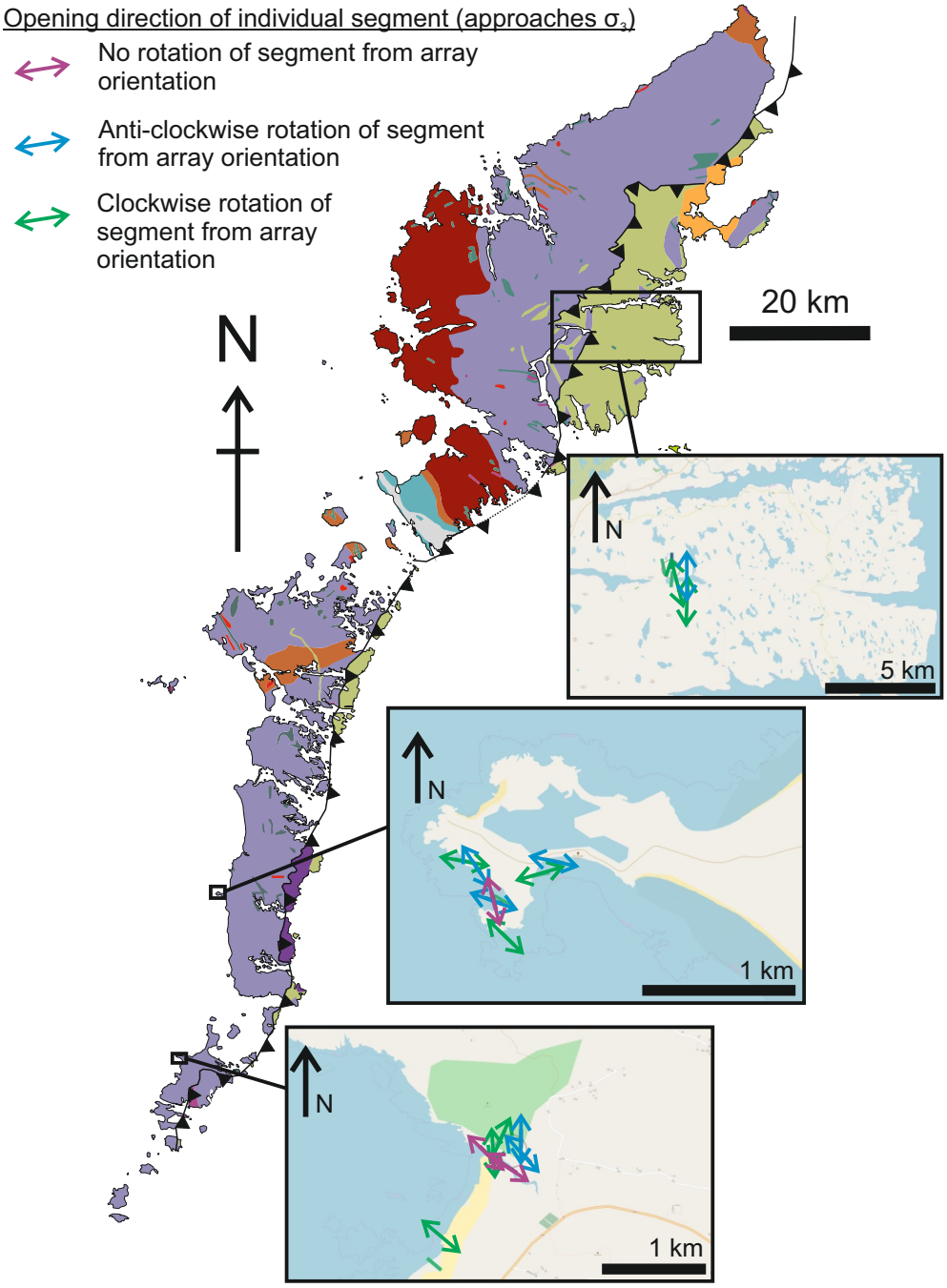
Opening direction of individual segment (approaches σ_3)
No rotation of segment from array orientation
Anti-clockwise rotation of segment from array orientation
Clockwise rotation of segment from array orientation
N
20 km
N
5 km
N
1 km
N
1 km

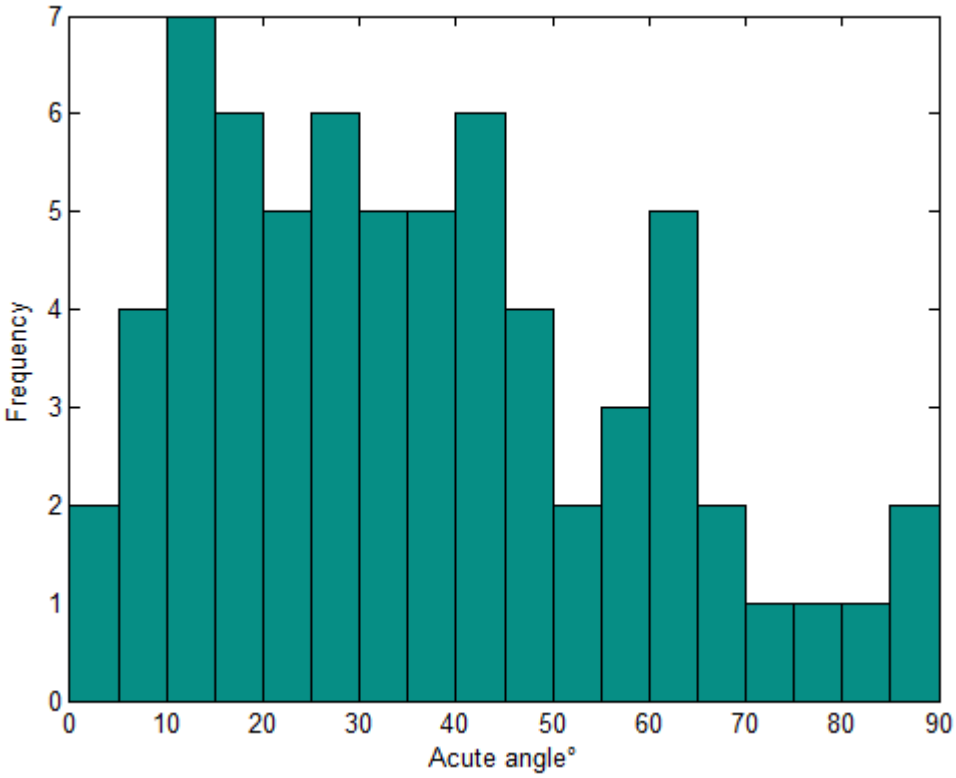
Frequency
Acute angle°
0
1
2
3
4
5
6
7
0
10
20
30
40
50
60
70
80
90

1. Possible pre-OHFZ events

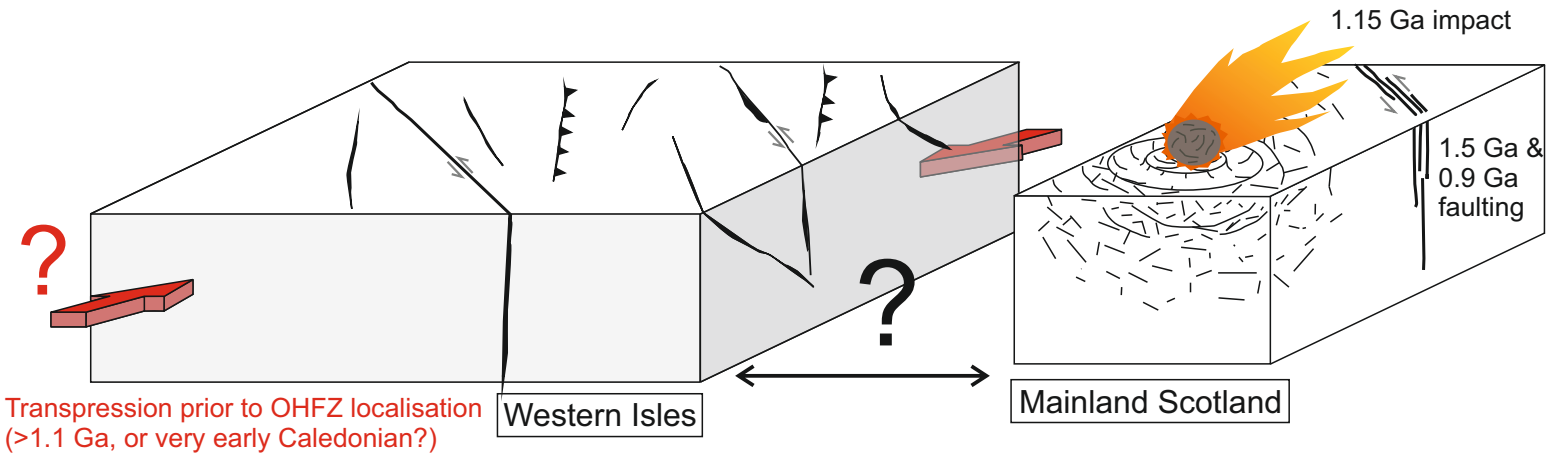

2. OHFZ faulting under variable stress fields